UNIVERSITY OF MICHIGAN & UNIVERSITY OF TWENTE

REPORT

Experimental research on two-phase mixing between two vertical channels connected through a gap

Authors
Zakaria TAZI HNYINE

June 15, 2017

Internship at the University of Michigan

Dpt. of Naval Architecture and Marine Engineering

U-M supervisor: ir. J.W. Gose
UT supervisors: prof. dr. ir. C.H. Venner
prof. dr. ir. H.W.M. Hoeijmakers

June 15, 2017

Zakaria Tazi Hnyine | s1354329

University of Michigan
222 Naval Architecture and Marine Engineering Building
2600 Draper Drive
Ann Arbor, MI 48109-2145
United States of America
tel. +1 734 764 6470

University of Twente
Master Mechanical Engineering
Drienerlolaan 5
7500 AE Enschede
The Netherlands
tel. +31 53 4 89 91 11

Number of pages of content: 62

UT/ME-June 15, 2017

Acknowledgements

I would like to thank Prof. Hoeijmakers from the University of Twente (UTwente) for arranging this internship for me, Prof. Ceccio from the University of Michigan (U-M) for the opportunity for me to attend the university for research, and James Gose from U-M for allowing me to participate in his research, for giving me hands-on experience doing experimental studies, having patience with me whenever I needed help, and for supervising me doing research in general. I would also like to thank Elisabeth Callison (U-M) for her assistance, and all organizations[1] who have sponsored this research.

---

[1] Their names are confidential.

Contents

List of Figures

List of Tables

Part 1: Experimental research

Chapter 1

Introduction

Inter-channel mixing through gaps is a process of mass transfer which naturally occurs in applications ranging from small household-size heating systems, to nuclear reactors, or any large industrial facility that requires heat exchange (e.g. a shell and tube heat exchanger). Mixing between different flow channels may occur due to natural or forced pressure differences between flow regions. Also, fluid from one channel may be entrained by turbulent flowing regions surrounding this fluid, introducing inter-channel turbulent mixing. Large structures from vortex shedding due to flow separation around blunt objects may be another cause means of this mixing, given a geometry allowing inter-channel vortex motion. Characterization of both single- and multi-phase mixing of flows between channels have been investigated in the past [1] - [8]. Furthermore, [9] has thoroughly performed a review on former studies related to interchannel mixing, where he found that periodic pulsations of large scale structures formed the main reason of the mixing process between gap-separated channels, where height and Reynold's number appeared to be the main factors influencing the mixing behavior, which e.g. [11] mentioned as well. [10] also studied this subject through numerical simulations, and found that near-gap regions retain high turbulent kinetic energy, which flow pulsations redistribute to other parts of the channel. These pulsations appear to be similar phenomena as those observed in the aforementioned studies, as well as in previous research performed in our own laboratory ([7]), and in various other studies ([13], [12], [6]). Researchers have performed a number of Computational Fluid Dynamics (CFD) studies on single-phase cross-channel mixing flow (e.g. [13], [12], [10] and [11]), yet few (mainly [14] and [8]) numerically analyzed interchannel turbulent mixing of multi-phase flows. Whilst little experimental research has been done on single-phase inter-channel turbulent mixing, even less has been accomplished for its multi-phase counterpart that can be employed for high-fidelity numerical modelling. Experimental research is often subjected to uncertainties, which must be identified in order for numerical simulations to properly model them. These uncertainties may stem from sources such as improper quantification of variables by the instruments used, or errors in the set inlet boundary conditions for the experiment – the sensitivity analysis of [15] shows that small pertubations in the inlet boundary conditions of flow could significantly influence mixing results, which makes proper characterization of uncertainties in the experimental setup of paramount importance for verification and validation of CFD simulations.

Therefore, Mäkiharju [7] closely quantified system parameters such as channel geometry and measurement uncertainties of in particular the inlet flow conditions for their inter-channel single-phase mixing through a narrow rectangular gap geometry, as to be able to perform high-fidelity CFD validation and verification. Building on this set-up, Mäkiharju's [7] research has expanded into a two-phase conditioned flow problem, which will be the center of discussion in this paper. System parameters such as liquid mass transfer and air bubble properties (e.g. bubble size and velocity) have been determined using fluorscein tracer dye concentration measurements resp. Wire-Mesh Sensors (WMS) at all four channel boundaries (i.e. two WMSs at the inlet and two at the outlet). Although these particular type of WMSs have been validated and used in various other studies already (for example see [16]), basic WMS validation has been performed through comparative analyses using high-speed imaging and flow sensors.

This paper will commence with a description of the experimental setup, in which we will go into detail about the system geometries, instruments and corresponding uncertainties. Then, the found results of mixing experiments performed at various gap heights, gas fluxes and Reynolds number will be shown, which afterwards will be analyzed further in the discussion, finally followed by the conclusions.

Chapter 2

Methods

2.1 Geometry

The experiments were carried out at University of Michigan's Marine Hydrodynamics Laborary (MHL) facility. See Figs. 2.1 and 2.2 for an overview of the experimental set-up. The test section consisted of two vertical channels (A and B) with hydraulic diameters D_h of $127\,mm$ that are connected through a gap that is $L = 1219.2\,mm$ long, $W = 228.6\,mm$ with a variable gap height of $H = [0, 50] \pm 0.1\,mm$. Beyond each channel outlet a weir box has been placed as to separate liquid from gas phase, and to provide a constant back pressure at the outlet by keeping its water level constant. As having visual recognition of phenomena helps in understanding flow behavior, the aluminum framework consisted of polished, optical grade acrylic windows. These windows allow high-speed imaging analyses through bubble and fluorescein dye tracking—this is a method utilized in this particular research—or particle image velocimetry (PIV), for example. The extent to which the windows facing the gap on the front and the rear are inserted into the frame depends on desired gap height, as four screws embedded in each of these two windows enable the adjustment of the gap height. In order for the flow to be symmetrical, it was imperative that we made sure both window ends (i.e. the place at which the gap 'begins') be equidistant from their corresponding aluminum frame walls. The root-mean-square surface roughness R_{RMS} of the inner walls was $1.5\,\mu m$.

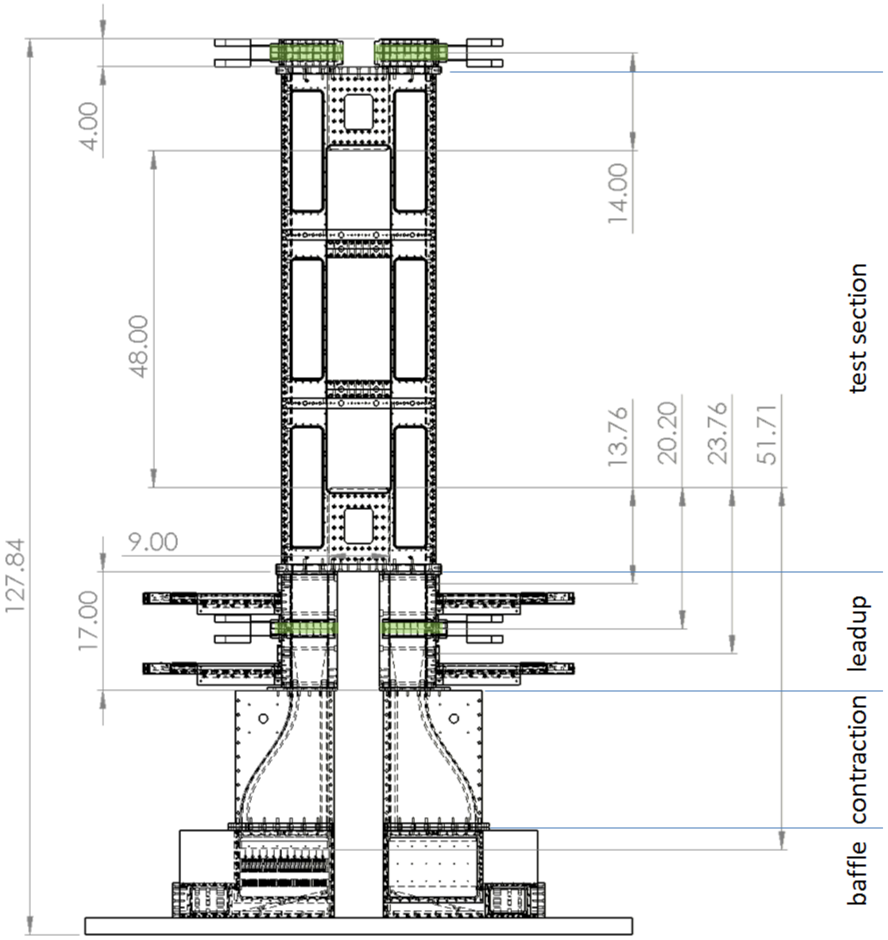

Figure 2.1: The geometry and dimensions of the test section. Both channels A (left) and B (right) had a hydraulic diameter,D_h, of 127 mm. The location of the WMS are shown in green. Dimensions shown are inches. *Courtesy of J.W. Gose.*

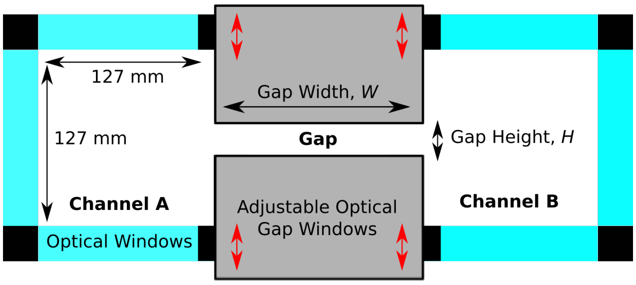

Figure 2.2: Schematic representation of the cross-section. *Courtesy of J.W. Gose.*

2.2 Equipment

2.2.1 Liquid flow sensors

Inlet and outlet mass flow rate sensors were measured using Krohne Optiflux 4000 electromagnetic flow meters and Krohne Optimass 1400 Coriolis flow meters respectively. The former had an IFC-300C signal converter with a specified accuracy of ±0.2% of measured value; the latter was specified to be accurate up to ±0.24% of measured value at $5.552 \times 10^{-3} m^3 s^{-1}$ and ±0.18% at $14.13 \times 10^{-3} m^3 s^{-1}$. Due to the possibility of gas entrainment in the outlet liquid flow pipes, a sensor that allowed for continuous measurement with 0 to 100% gas entrainment had been chosen at the outlets. These accuracies were verified during closed-gap flow measurements, where the water level of the storage tank was closely monitored, whilst no liquid mass was being added into the reservoir.

2.2.2 Air flow sensors

Air was injected at both channel inlets at a distance of $\Delta L = 12D_h$ upstream of the mixing gap by means of two types of needle arrays, one having a inner diameters of $102^{+25}_{-13}\,\mu m$, and outer diameters of $229^{+13}_{-0}\,\mu m$; the other having inner diameters of $508^{+25}_{-13}\,\mu m$ and outer diameters of $635^{+13}_{-0}\,\mu m$.The air flow rates at the inlet channels were measured using Bronkerhorst F-202AV-M10-AGD-55-V, a digital mass flow controller which can measure air flow rates between 3 and 150 slpm with a manufacturer specified accuracy of ±0.5% of measured value plus ±0.1% of full scale. At the outlets, Sierre 640S thermal mass flow meters that capture fluxes between 0 and 400 slpm with a manufacturer specified accuracy of ±1% of measured value plus ±0.5% of full scale reading were used. The needle valves were assembled into four 6×6 arrays, two per channel inlet. Another way of determining air flow rate was through the use of Helmholtz-Zentrum Dresden-Rossendorf's manufactured wire-mesh sensors (WMSs), of which the reliability will be discussed later on. A set of two WMSs were placed at the inlet and outlet of both channels, spaced $50\,mm$ apart. The second WMS allows for a velocity measurement by determining cross-correlating bubbles passing through subsequent WMSs, which was done by running built-in code embedded in the 'Wire-Mesh Sensor Framework' software package written by HZDR. Moreover, we do acknowledge the intrusive behavior of the WMS on the bubbles passing through. We have measured a decrease in bubble size of around 20 to 40 percent as a result of the wires breaking up the bubbles. It is also worth noting that bubbles with diameters smaller than 2.5 mm may pass the WMSs without getting registered.

2.2.3 Pressure sensors

An Omega Engineering DPG409-030A pressure transducer was used for measuring the absolute pressure in the channels within a range of 0 to 207 kPa ±0.08% of full scale.

Across the inlet and outlet channels a Dwyer 3100D differential pressure sensor enabled measurements between -2.49 to 4.98 kPa ±0.075% of full scale, having additional Rosemount 3051 CD differential pressure transducers installed that measure the pressure differentials (i.e. pressure drop) between both in- and outlets with a range of 0 to 25 kPa and a manufacturer specified accuracy of ±0.04% of full scale. Furthermore, two manometers with an estimated accuracy of ±7.5 Pa were installed in order to read the pressure differentials between the channels at two different locations. Next to mass flow (i.e. velocity) and pressure, another important physical variable for determine flow characteristics (e.g. viscosity) is the temperature, which was continuously measured through four Omega Engineering P-M-A-1/4-6-0-P-3 4-wire $100\,\Omega$ platinum RTD sensors.

2.2.4 Dye sensors

In addition, in order to measure inter-channel mixing, a fluorometer has been set into place next to the test section, which connects with the channel inlets and outlets using plastic tubes. Fluorescein sodium salt has been measured using Turner Designs CYCLOPS-7 (C7) Submersible Fluorometer, PN 2100-000/2108-000-F Fluorescein Dye (serial number 2180463). The uncertainty of the measurements using this sensor were ±0.5% of reading, with an additional $\pm 1\,ppb$. These uncertainties were manufacturer specified. As for the setup, one tube connected inlet channel A with C7, another inlet channel B, while three other tubes connected outlet channel A at the position at the position of the weirboxes—*three* were positioned horizontally spaced, as to prevent measurement of unequally mixed liquid-dye blobs at the outlets. A sixth tube connected B outlet with the C7 sensor; a seventh with a fresh water tank, which flushes the sensor every time a valve to one of the channel positions—know that only one valve can be opened at a time: the sensor has got room for one input position only—in order to avoid dye contamination from previously opened channel positions.

2.2.5 Imaging

Another way of characterizing bubbles is by taking high-speed camera (HSC) footage of a running experiment, processing it in MATLAB and comparing bubble sizes to the ones found using the wire-mesh sensors. These data could be used to compare WMS data with, although strong limitations prevented us from doing this comprehensively (that is: 'accurately' and 'for all taken test cases'). The camera used was a Basler acA200-340kc, with a Kowa 6mm f/1.8-16 lens. This camera has a CMV2000 sensor that is 11.26 mm × 5.98 mm. The camera has a resolution of 2046×1086 pixels and can record at a maximum of 60 fps.

2.2.6 On unused equipment

Before elaborating on the procedure of taking mixing data, I would like to also briefly mention one of the goals we had set at the beginning of the internship, but has not been reached due to external factors. I commenced the internship by taking validation measurements from the wire-mesh sensors and high-speed cameras first (the latter in collaboration with a lab partner), as to be sure the data we were obtaining were trustworthy in the first place. I will go into this in more detail in section 2.3. Another way of validating wire-mesh sensor data was by comparing those to measurements taken by dual-tip optical probes (OP). These probes, manufactured by the French company *RBI Instrumentation*, measure either vapor or liquid due to differences in refraction indices of the medium around the optical probe's fiber tip, as intensity of light-reflection through the probe changes as a result. With these in place, we could take measurements and verify bubble size and velocity data using WMSs, HSCs and OPs. Unfortunately, after almost of testing, calibrating and trying to repair the OPs, we concluded that they had to be sent back to their manufacturers for repair. For more information, see Appendix A for a succinct report on the OP problem. During the internship, it would appear that the probes would not be sent back until the second-last week of my stay at U-M. It is not until after my leave that the probes are finally used.

2.3 Experimental procedure

2.3.1 Running the experiment

Before running the experiment, several 'checks' have to be performed. Water used for the experiment is stored in a large tank (the 'wave tank') that is approximately $35 \times 0.55 \times 0.70$ (in meters, $L \times W \times H$) (approximately 13,500 liters). Because this tank is also used for other types of research, one must make sure the valves that connect the tank with the test section are opened, and that the water level in the tank is at the correct height. We constantly added a stream of fresh water into the tank and drained water out at the same time as well. As fluorescent dye is injected in channel B's input pipe, runs through the test section and pumped back into the tank, adding fresh water, removing old water, and maintaining a certain water level helps in decontaminizing the water tank. Approximately 170 ppm of fluorescein was injected into channel B, a little less than half a meter upstream of the pump that channels water into B. Another measure taken to keep the tank's dye concentration as low as possible, is by adding chlorine to the tank at the start of each experiment. The chlorine was dispensed via a drip dispenser (which was basically a bucket with a small hole). After a run, it usually took an hour for the chlorine to reach most of the fluorescein. Only when the concentration has dropped sufficiently, another run could be performed. See Fig. 2.3 for a simplified overview of the loop.

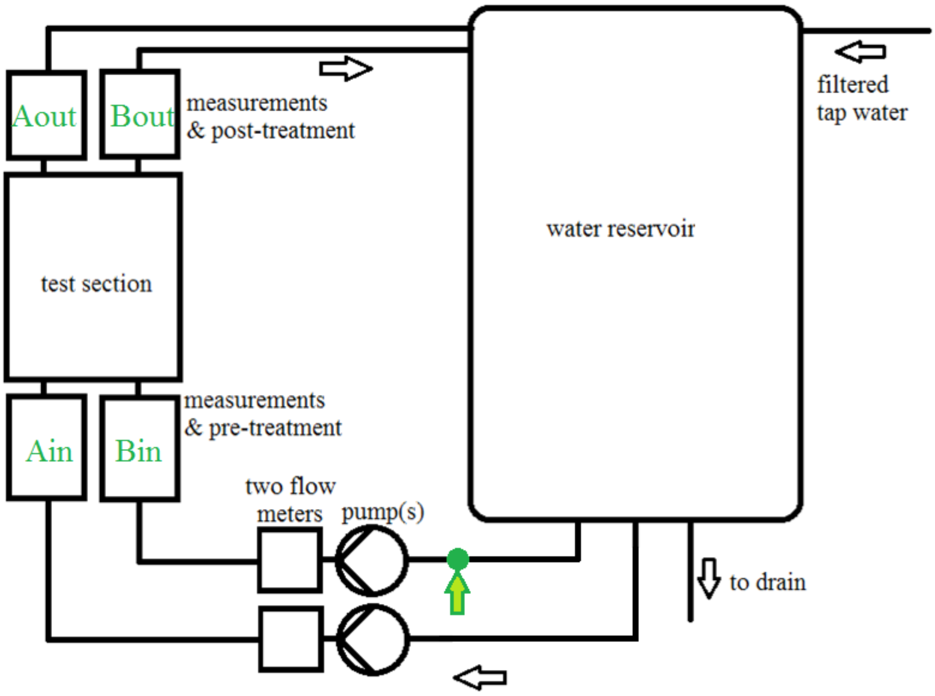

Figure 2.3: Simplified overview of the flow loop, where the green dot denotes the position of dye injection. A_{in}, A_{out}, B_{in} and B_{out} indicate sampling locations. *Courtesy of J.W. Gose.*

Next, we need to make sure the pressure at the two weir boxes (at the top of the test section) remains constant. At each channel outlet, a box has been connected in which water builds up and overflows into a larger tank space (from which water is pumped out and sent back into the wave tank). The weir boxes facilitate phase separation: gas floats up; water flows over the box ridge. We maintainted the weir box pressure at between approximately 0.3 m and 0.4 m of water in order to provide a constant back pressure to the test section flow. These tank levels are kept constant by balancing and adjusting the rotation frequencies of the in- and output water pumps of both channels until a semi-steady state is reached. Everything is monitored manually, which allows for human error: when in- and outputs are uneven, water levels may significantly rise, until it fills up the weir box tank entirely. Pressure will build as a result, which would likely lead to serious damage as weak pipe sections will succumb to these high stresses. It was therefore paramount to always have someone monitor tank levels whenever the facility was running. Furthermore, whenever we first turn on the pumps, excess air needed to be removed before being able to take data. This was simply a matter of waiting until no more air enters the test section through the liquid flow pipes. Valves at the upper side of the liquid inlet pipes could be opened in order to prevent air from coming into the section, and lead it to a sink instead. You do not want air from the pipes to meddle with the bubbles of the controlled gas fluxes you inject.

Now water flows in and out in a balanced matter, water and air are separated at the top (so only water is pumped back into the tank), and the weir pressures are appropriate, we need

Table 2.1: Experimental parameters

Re (-)	Gas flux (slpm)	Gap (mm)
$4 \cdot 10^4$	[0, 10, 20, 50, 100, 150]	[0, 20, 50]
$6 \cdot 10^4$	[0, 10, 20, 50, 100, 150]	[0, 20, 50]
$8 \cdot 10^4$	[0, 10, 20, 50, 100, 150]	[0, 20, 50]
$1 \cdot 10^5$	[0, 10, 20, 50, 100, 150]	[0, 20, 50]

to make sure that the dye concentrations in the water are sufficienctly low. The fluorometer can not measure concentrations of 'infinite' height: it has a maximum. Therefore, we needed to make sure that we would start at a sufficiently low concentration, and that adding dye did not lead to concentrations too high. The fluorometer was connected to the computer, which displayed concentration values (in Volts) in semi-realtime. If concentration levels were too high still, we either waited until they subdued, increased the wave tank water level, drained more 'old' water, or added more chlorine to the tank. We usually waited. Adding more chlorine was not something done often, as that may break up fluorescein even within the space of the vertical test section. We examined whether break-up took place over the test section, by checked the mass balance of the dye coming in and dye going out (see Eq. 2.1).

$$\dot{m}_{ai}C_{ai} + \dot{m}_{bi}C_{bi} = \dot{m}_{ao}C_{ao} + \dot{m}_{bo}C_{bo} \tag{2.1}$$

Furthermore, as both air and water enter the tubes that connect the channels with the C7 sensor, and dye can only be contained in the liquid, we need to separate gas and liquid, so that only liquid enters the fluorometer. It was *crucial* that this phase separation took place. More than once, making sure the fluorometer works as needed was forgotten, which required us to redo the experiment (one experiment would cost us approximately one hour (set up, do 'checks', and run)). After starting the experiment, one must walk to the dye injection system (which is outside the room where the test section is placed), turn it on as data is being sampled, and turn it off the moment the sampling finishes (after 20 or 13 minutes).

Further, when everything else has been checked, when the sensors display the values you expect them to display, you can now start the measurement. If adding bubbles is part of the experiment (it usually is: we performed more two-phase than single-phase flow measurements), then you should open the gas valves and inject air at a flow rate of your desire. Again, it is important to check whether the sensors measure values which resemble the gas flux you put in.

As a final remark, because experiments are taken at different gap widths, the desired gap height had to be fixed before pumping in water. Because only two different gap heights were examined for the experiment (i.e. 50 mm and 20 mm gaps), this only had to be done twice over several months. See Table 2.1 for an overview of the experiments done.

2.3.2 Taking WMS data and .tdms data

Once everything was up and running, data which the researchers called *WMS* and *.tdms* data had to be collected (taking HSC data will be discussed in the next subsection). The length of a 'run' was usually determined by the amount of time before dye recirculates into the facility. Injecting dye into the facility will make it so that dye-mixed water gets pumped back into the wave tank, and eventually recirculates into the facility if waited long enough. Depending on the liquid flow rates used, circulation time changes. For runs at liquid flow rates $\dot{Q}_l$ of 81 gpm to 161 gpm (0.0051 m^3s^{-1} to 0.010 m^3s^{-1}), a twenty-minute run was shown to be suitable. For $\dot{Q}_l = 201$ gpm, measurement times had to be reduced to 13 minutes. Valve sampling at the different channels by the C7-sampler had to be reduced doing that. C7 data is part of what is called .tdms data. The following relevant quantities are measured and stored in a .tdms-file:

- Gas fluxes $\dot{Q}_{gFM,i}$ with $i = [ai, bi, ao, bo]$, denoting the channel locations A & B and 'in' & 'out'. 'FM' stands for 'flow meter';
- Liquid fluxes $\dot{Q}_{l,i}$;
- Channel pressures p_{bi}, p_{abi}, p_{abo}, p_{bio}, where i means 'in', ab the pressure differential between A and B, and io the pressure differential between 'in' and 'out'.
- Fluorometer voltages f_V;
- Fluorometer gain values f_G;
- Fluorometer valve signal f_{sig};
- Water temperatures T

The quantity f_{sig} indicates which valve is being sampled at a certain point in time. Dye sampling is 'scheduled' to behave according to the following scheme *([valve signal value] ([time in seconds]))*:

$$\begin{aligned} &0(50) \rightarrow 1(50) \rightarrow 3(100) \rightarrow 1(50) \rightarrow 4(100) \rightarrow 1(50) \rightarrow 5(100) \rightarrow 1(50) \\ &\quad \rightarrow 7(100) \rightarrow 1(50) \rightarrow 9(100) \rightarrow 1(50) \rightarrow 10(100) \rightarrow 1(50) \rightarrow 3(100) \end{aligned}$$

where:

- 1 is fresh water flush;
- 3 is channel ai;
- 4 is channel ao (left);
- 5 is channel ao (middle);
- 7 is channel ao (right);
- 9 is channel bo;

- 10 is channel bi.

See Fig. 2.4 for a quick overview.

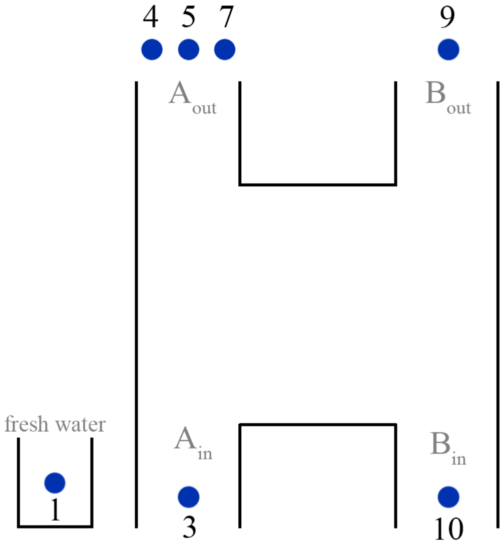

Figure 2.4: Simplified schematic of dye sampling locations.

For the $\dot{Q}_l = 121\,gpm$ case, the following scheme was used:

$$0(50) \to 1(30) \to 3(75) \to 1(30) \to 4(75) \to 1(30) \to 5(75) \to 1(30) \\ \to 7(75) \to 1(30) \to 9(75) \to 1(30) \to 10(75) \to 1(30) \to 3(75)$$

The rest of the data did not reduce in size: I only reduced the measurement time of the fluorometer. Obviously, recirculation of dye did not prevent us from taking e.g. pressure measurements.

Furthermore, during a run, WMS data had to be taken as well. For each data run, four WMS measurements had to be taken (that is at ai, bi, ao, and bo). Because there was only one set of WMS connector cables available, we had to disconnect and reconnect cables to the different WMS boxes during the experiment every time. One WMS measurement covered thirty seconds of data. We assumed bubble properties (velocity, size, void fraction) to be time invariant, so did not take measurements longer than that. Moreover, processing thirty seconds of WMS data of a single run takes around twenty minutes. One single data run (four sensors, so four WMS measurement files) takes around an hour to fully process. Note: with 'processing WMS data', we mean using the WMS Framework software to convert the measurement files into files containing directly usable information: for example, one of the things needed to be done was substracting a calibration measurement file (a zero-gas flux case measurement) from the data run measurement files. So save time and reduce human error, the largest part of this process has been automated using MATLAB. Processing WMS data for one case—we looked at five different gas fluxes per Reynolds number (i.e. a 'case')—would usually take at least seven hours to process using

MATLAB alone. The manual preparations needed before that cost several hours as well. See below for a short description of 'processing WMS data'.

Processing WMS data

1. Add information to EXCEL file (data run number, length of measurement, frequency, channel location, etc.).
2. Open WMS Framework software.
3. Add and convert the *.mes files to *.dat files. (*.mes files are obtained directly from the WMSs.)
4. Subtract *.dat calibration files from *.dat files.
5. Move *.dat files and resulting files[1] to a different folder (that is the MATLAB folder).
6. Run MATLAB code.
7. Obtain files[2] for post-processing.

2.3.3 Taking HSC data

Next to taking WMS and .tdms data, we also retrieved bubble data using the HSCs. Albeit limited in utility—gas fluxes of only 5 to 20 slpm could be analyzed (with a large error still)—these obtained properties could be compared to those found using the WMSs, and so be used for validation. At least, that was the idea. We will later find out that the MATLAB code could not properly identify individual bubbles, which lead to large errors in predicting bubble quantity and size.

After positioning the camera in its desired position, calibration images had to be taken first. This 'calibration' involves removing a side-window of the test section, inserting a ruler with its numbers facing the camera and taking a snapshot. Now we know how many pixels on screen represent one millimeter in the test section, we can count the bubble sizes in pixels and convert them to a different length unit. The difference in pixel-to-millimeter ratio was negligible in the depth of $(\frac{1}{2})127$ mm of the cross-section.

For each low gas flux case, a set of 700 consecutive frames were taken at a rate of 60 fps. These images were then imported into MATLAB, which then tried to identify individual bubbles by compiling the (black-and-white) images into a video, increasing the contrast to 100 % (so only two colors were left), and searching for bubble kernels and their respective outer boundaries. The next chapter will demonstrate the results of these computations being rather imperfect.

---

[1] *.epsxy files giving time-averaged void fractions per wire crossing; *.epst files giving cross-section averaged void fractions over time; *.a files giving bubble properties (e.g. quantity, radii)

[2] *.his_lin files giving histogram of bubble diameters; *.velxy files giving time-averaged bubble velocities per wire crossing

2.4 Post-processing

After having obtained raw data and having processed these into 'usable' raw information, it was then needed to obtain desired quantities which characterize mixing behavior and those that influence mixing.

Remark: this experimental research has been done without exactly knowing which quantities influence mixing really, or which combination of quantities could be used to characterize mixing behavior. In all fairness, we 'tried' combining different quantities together, plotting several different quantities against mixing behavior, and did not get anything 'really' useful (or anything we did not know already). Therefore, you might notice that some quantities will be introduced in the methods section that you will not see in the discussion chapter later on. The reason I introduced them nevertheless is to try to provide the reader a more realistic image of doing experimental research.

2.4.1 WMS and .tdms data

Velocities

When looking at bubble velocity data, we noticed that it contained unrealistically high valued spikes (over 100 m/s) at random positions on the $x-y$ grid (note: z is the direction of the flow). These velocity files were created by cross-correlating data of bubbles passing through the first and second sensor—as mentioned before, each channel location had two sensors installed 50 mm apart in the direction of the flow, i.e. 'one above the other'. The bottom sensor is called 'sensor 1'; the upper 'sensor 2'. The WMS Framework software obtained the velocities by calculating cross-correlation values, defined as:

$$F_{i,j,\Delta k} = \frac{\sum_k \varepsilon'_{1,i,j,k} \cdot \varepsilon'_{2,i,j,k+\Delta k}}{\sqrt{\sum_k \varepsilon'^2_{1,i,j,k}} \cdot \sqrt{\sum_k \varepsilon'^2_{2,i,j,k}}} \tag{2.2}$$

where

- i is the spatial index in the x-direction;
- j is the spatial index in the y-direction;
- k corresponds to the time; Δk to the time-shift of $\Delta t = \Delta k / f_{meas}$. We set $f_{meas} = 3200\,Hz$;
- $\varepsilon'_{i,j,k}$ is the void fraction fluctuation: $\varepsilon'_{i,j,k} = \varepsilon_{i,j,k} - \bar{\varepsilon}_{i,j}$.

Afterwards, it searched for the k-indices corresponding to the highest cross-correlation value per node over the time measured, and used it for calculating the velocity:

$$v_g(x,y) = \frac{\Delta L}{\Delta k_{max}} \cdot f_{meas} \tag{2.3}$$

where ΔL is the axial distance between the two sensors (i.e. 50 mm in our case).

Going back to the problem we encountered (the velocity peaks), we found that the cross-correlation values were extremely low: they did not even top values of 0.4. Most cross-correlation values were found to be between 0.1 and 0.2, which obviously is extremely low to base your velocity calculation on. The fastest solution to this problem we took on was by simply looking for the spikes, and averaging them out locally. We attempted to 'solve' this problem by going through several different measure to remove the peaks. In general, our solution looked as follows (v_G is simply v now):

$$\text{if } v_{i,j} > v_{threshold} \text{ then}$$
$$v_{i,j} = v_{new}$$

where we make v_{new}

$$\boxed{v_{new} = \frac{v_{i-1,j-1} + v_{i,j-1} + v_{i+1,j-1} + v_{i-1,j} + v_{i+1,j} + v_{i-1,j+1} + v_{i,j+1} + v_{i+1,j+1}}{8}} \tag{2.4}$$

using a grid like in Fig. 2.5, just like the way WMS wires are aligned (and that is the most obvious choice for a grid).

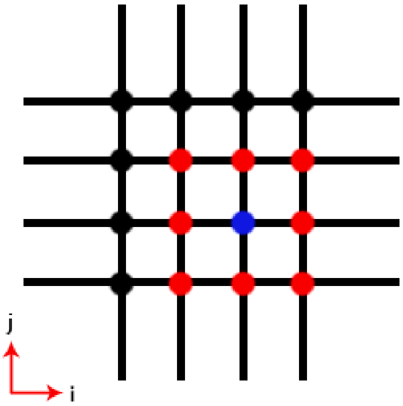

Figure 2.5: Grid used to average peak-velocities locally. Blue: peak velocity. Red: area used to take on new grid value.

The threshold velocity (meaning the minimum velocity at which velocity adjustment will take place) has been set to be: $v_{threshold} = Av^p_{water} + Bv^q_{G,i,j}$, with $A = 6$, $B = 1$, $p = 2$, and $q = 2$. These values were obtained by trying to optimize the percentual difference between the gas flux we know (i.e. the one coming from the gas flow meters: Q_{gFM}) and the gas flux calculated using the velocity data from the WMSs:

$$Q_{gWMS} = \bar{\varepsilon} A_{channel} \bar{v}_{gWMS} \tag{2.5}$$

where $\bar{\varepsilon}$ denotes the average void fraction of a sensor (that is either sensor 1 or 2), $A_{channel}$ the cross-sectional area of the channel ($A_{channel} = 0.127^2$), and $\bar{v}_g$ the average bubble velocity measured by the WMS. When looking for values for A, B, p and q, we optimized (minimalized) for:

$$ratio = \frac{Q_{gWMS} - Q_{gFM}}{Q_{gFM}} \tag{2.6}$$

With the aforementioned parameter values, we could obtain a ratio of around 0.15, and used that for future post-processing. Mind you, this is more 'coping with bad-functioning sensory equipment' than it really is 'solving' the problem. Solving the problem would mean not having to adjust incoming data at all. It has been suggested to place the WMSs closer together—just a couple of millimeters instead of 50—as to enhance cross-correlating the data. The reason we did not do this during my period there, was because of the difficulty of removing the WMSs, and the pressing time constraints. I did try removing it myself, but the WMS box has been too tightly connected to the test section. Still, the WMSs will have to be removed in the future in order to allow for more accurate measurements in further studies.

Drift flux

One way of characterizing two-phase flows is by regarding the flow as a more homogeneous structure using the 'drift flux model'. The mixture as a whole is considered. The drift flux is the flux of the gas relative to a plane moving at the total superficial velocity, so it assesses the relative motion of the two phases. The gas phase is transported at the drift velocity with respect to the mixture velocity. To obtain these 'relative velocities', we first need to obtain the total combined superficial velocity of the two-phase flow. The separate superficial velocity components are defined as given in Eqs. 2.7 and 2.8. It is important to understand that even though we could use the drift flux for characterizing the flow, the void concentration and superficial velocity profiles can still vary independently of one another.

$$j_g = \varepsilon v_g \tag{2.7}$$

$$j_l = (1 - \varepsilon) v_l \tag{2.8}$$

Then it follows that the total mixture superficial velocity is simply the sum of the two:

$$j = j_g + j_l \tag{2.9}$$

For these calculations, we need WMS data (the void fraction and bubble velocity). We could also use the information we get from the flow meters:

$$j = \frac{Q_g + Q_l}{A_{channel}} \tag{2.10}$$

In MATLAB, we calculated these drift quantities based on the cross-sectional averaged void fractions (denoted using the $\langle ... \rangle$-bracket) and velocities (i.e. $\bar{\varepsilon}$, $\bar{v}_g$ and so on). The velocity $\bar{v}_g$ can be obtained directly using the WMs only, or by using void fraction data from the WMSs and liquid flowrate data from the .tdms-files:

$$\bar{v}_g = \frac{Q_g}{\langle \varepsilon \rangle A_{channel}} \tag{2.11}$$

The local gas phase drift velocity is obtained by substracting the total superficial velocity from the local gas phase velocity:

$$v_{gj} = v_g - j \tag{2.12}$$

Finally, the void-fraction-weighted cross-sectional averaged drift velocity is defined as

$$\bar{v}_{gj} = \frac{\langle \varepsilon v_{gj} \rangle}{\langle \varepsilon \rangle} \tag{2.13}$$

which gives a more accurate representation of the drift velocity when regarding the entire cross-section.

Mixing

The mass transfer coefficients of water and air through the gap was determined assuming mass conservation for the water, air, and fluorescent dye (which has been dissolved into the water before it entering channel B). The mixing process is schematically shown in Fig. 2.6. The single-phase mixing for the current test geometry has been fully characterized by [7]. That research showed that small gap heights ($< 8\,mm$) lead to no significant leakage (i.e. mixing or gross mass transfer) between the two channels. For larger caps, it did; coherent structures similar to those reported in earlier studies (see the introduction chapter) were observed. Visual observations from the authors stated that these large vortices arose from a Kelvin-Helmholtz type instability, occuring with regular temporal frequency. They also noted that the balanced flow mixing appeared to be independent of the Reynolds numbers over the parameter range investigated. In this work we replicated the single-phase work of [7] to measure the fluorescein dye tracer concentration, C, to confirm the baseline and extended the approach for the multi-phase mixing characterization. We obtained the 'true' voltages from the fluorometer through Eq. 2.14.

$$f_{V,true} = \frac{f_V}{f_G} \tag{2.14}$$

where the voltages were converted to concentrations C using the following calibration function:

$$C(x) = \begin{cases} 1.77x^2 + 66.459x - 0.4541 & x \leq 3.2 \\ 71.176x^2 - 364.8x + 668.63 & x > 3.2 \end{cases}$$

For x we filled in $f_{V,true}$.

The integral mixing coefficients denoted as x and y were calculated to determine the fraction of liquid leakage from channel A transferred to channel B and from channel B transferred to channel A, respectively. This is what we will call 'mixing'. The mixing coefficients were determined using conservation of mass of the water and tracer using the three test section control volumes shown in Fig. 2.6. From the global control volume AB conservation of mass yields easily derived equations, Eqs. 2.15 and 2.16, where $\dot{m}$ is the liquid mass flux. Again, 'ao' means channel A outlet, 'bo' channel B outlet, and so on.

$$\dot{m}_{ao} + \dot{m}_{bo} = \dot{m}_{ai} + \dot{m}_{bi} \tag{2.15}$$

$$\dot{m}_{ao}C_{ao} + \dot{m}_{bo}C_{bo} = \dot{m}_{ai}C_{ai} + \dot{m}_{bi}C_{bi} \tag{2.16}$$

As for the mass conservation equations for control volumes A and B, we can derive the following:

$$\dot{m}_{ao} = (1-x)\cdot\dot{m}_{ai} + y\cdot\dot{m}_{bi} \tag{2.17}$$

$$\dot{m}_{bo} = x\cdot\dot{m}_{ai} + (1-y)\cdot\dot{m}_{bi} \tag{2.18}$$

In the two equations above, the former denotes mass conservation for control volume A; the latter for B. The same can be done for the dye concentrations, by simply adding their respective dye concentration components:

$$\dot{m}_{ao}C_{ao} = (1-x)\cdot\dot{m}_{ai}C_{ai} + y\cdot\dot{m}_{bi}C_{bi} \tag{2.19}$$

$$\dot{m}_{bo}C_{bo} = x\cdot\dot{m}_{ai}C_{ai} + (1-y)\cdot\dot{m}_{bi}C_{bi} \tag{2.20}$$

Using these equations (Eqs. 2.17 - 2.20), we can solve for x and y in different ways, all of which will be used to calculate these mixing coefficients with. The average will be taken eventually (and it will be seen that they will not differ that much). I will do one derivation here; the rest will be similar in nature. We will use Eqs. 2.17 and 2.19 in this example.

$$\rightarrow y = \frac{\dot{m}_{ao} - (1-x)\cdot\dot{m}_{ai}}{\dot{m}_{bi}} \tag{2.21}$$

$$\rightarrow \dot{m}_{ao}C_{ao} = (1-x)\cdot\dot{m}_{ai}C_{ai} + \dot{m}_{bi}C_{bi}\frac{\dot{m}_{ao} - (1-x)\cdot\dot{m}_{ai}}{\dot{m}_{bi}} \tag{2.22}$$

$$\rightarrow \dot{m}_{ao}C_{ao} = (1-x)\cdot\dot{m}_{ai}C_{ai} + C_{bi}\frac{\dot{m}_{ao} - (1-x)\cdot\dot{m}_{ai}}{1} \tag{2.23}$$

$$\rightarrow \dot{m}_{ao}C_{ao} = \dot{m}_{ai}C_{ai} - x\cdot\dot{m}_{ai}C_{ai} + \dot{m}_{ao}C_{bi} - \dot{m}_{ai}C_{bi} + x\cdot\dot{m}_{ai}C_{bi} \tag{2.24}$$

$$\rightarrow x\cdot(C_{ai} - C_{bi}) = -\frac{\dot{m}_{ao}}{\dot{m}_{ai}}C_{ao} + C_{ai} + \frac{\dot{m}_{ao}}{\dot{m}_{ai}}C_{bi} - C_{bi} \tag{2.25}$$

$$\rightarrow x\cdot(C_{ai} - C_{bi}) = \frac{\dot{m}_{ao}}{\dot{m}_{ai}}(C_{bi} - C_{ao}) + (C_{ai} - C_{bi}) \tag{2.26}$$

$$\tag{2.27}$$

This eventually gives for mixing from A to B and B to A respectively:

$$\boxed{x_1 = 1 + \frac{\dot{m}_{ao}(C_{bi} - C_{ao})}{\dot{m}_{ai}(C_{ai} - C_{bi})} \qquad y_1 = \frac{\dot{m}_{ao}(C_{ai} - C_{ao})}{\dot{m}_{bi}(C_{ai} - C_{bi})}} \tag{2.28}$$

We can use other combinations of the aforementioned equations to obtain the following expressions for the mixing coefficients:

$$x_2 = \frac{\dot{m}_{bo}(C_{bi} - C_{bo})}{\dot{m}_{ai}(C_{ai} - C_{bi})} \qquad y_2 = 1 - \frac{\dot{m}_{bo}(C_{ai} - C_{bo})}{\dot{m}_{bi}(C_{ai} - C_{bi})} \tag{2.29}$$

$$x_3 = \frac{\dot{m}_{ao}C_{bi} - (\dot{m}_{ai} + \dot{m}_{bi})C_{bi} + \dot{m}_{bo}C_{bo}}{\dot{m}_{ai}(C_{ai} - C_{bi})} \qquad y_3 = \frac{(\dot{m}_{ao} - \dot{m}_{ai})C_{ai} - \dot{m}_{bi}C_{bi} + \dot{m}_{bo}C_{bo}}{\dot{m}_{bi}(C_{ai} - C_{bi})} \tag{2.30}$$

$$x_4 = \frac{\dot{m}_{ai}C_{ai} - \dot{m}_{ao}C_{ao} + (\dot{m}_{bi} - \dot{m}_{bo})C_{bi}}{\dot{m}_{ai}(C_{ai} - C_{bi})} \qquad y_4 = \frac{(\dot{m}_{ai} + \dot{m}_{bi} - \dot{m}_{bo})C_{ai} - \dot{m}_{ao}C_{ao}}{\dot{m}_{bi}(C_{ai} - C_{bi})} \tag{2.31}$$

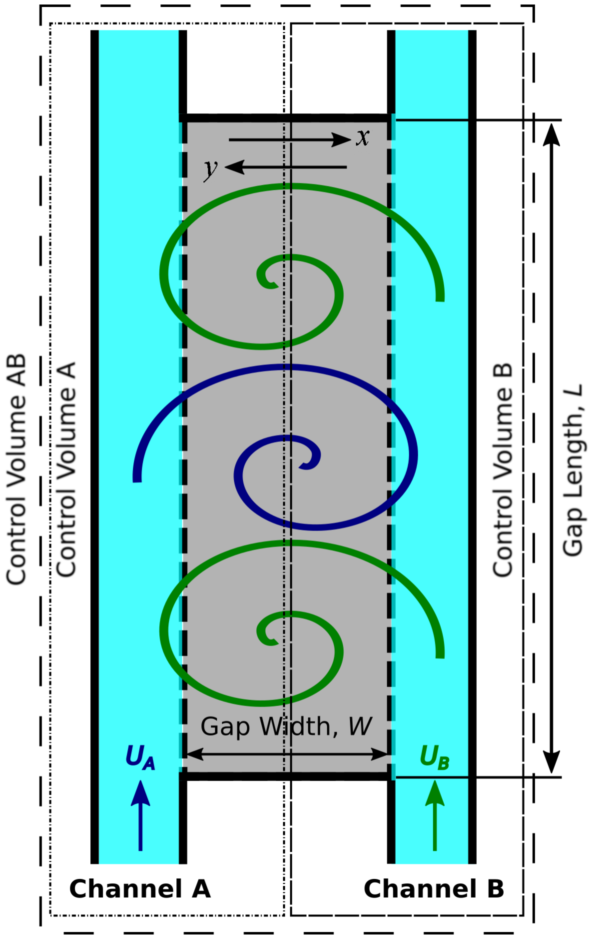

Figure 2.6: Schematic representation of large vortex shedding depicting the primary source of its mixing behavior. Water containing fluorescent dye enters through channel B, whilst 'uncontaminated' water (i.e. free of dye) enters channel A. *Courtesy of J.W. Gose.*

Future results will only show averaged mixing coefficient values $x = \frac{x_1+x_2+x_3+x_4}{4}$ and $y = \frac{y_1+y_2+y_3+y_4}{4}$.

Other quantities

Another computed quantity we used was the volumetric quality β, which is the volumetric ratio of gas to total flow flux.

$$\beta = \frac{Q_g}{Q_g + Q_l} \tag{2.32}$$

Also, the Reynold's number has been used throughout the research, taking the following are our baseline:

$$Re_{Dh} = \frac{\rho_l \tilde{v}_l D_H}{\mu_l} \tag{2.33}$$

where $\tilde{v}_l$ is defined calculated using the inlet flow conditions: $\tilde{v}_l = Q_{l,in}/A_{channel}$, D_H is the channel's hydraulic diameter, and μ_l the viscosity of the water, which depended on the temperature:

$$\mu_l = A \cdot 10^{\frac{B}{T-C}} \tag{2.34}$$

where $A = 2.414 \cdot 10^{-5}\, Pa \cdot s$, $B = 247.8\, K$, and $C = 140\, K$.

Other quantities used in the analysis during our research are the momentum fluxes, which we will calculate as (assuming z-direction flow only):

$$\text{Momentum flux gas} = \rho v_g^2 = \rho \frac{Q_g^2}{\varepsilon A_{channel}} \tag{2.35}$$

$$\text{Momentum flux liquid} = \rho v_l^2 = \rho \frac{Q_l^2}{(1-\varepsilon) A_{channel}} \tag{2.36}$$

Error analysis

All experimental research is prone to errors. All measurements of pressure, temperature, flow, etc. contained random errors, which were effectively eliminated by taking the mean of over 100,000 samples each run. As for the known manufacturer specified errors, we included these in our analyses of the quantities as follows

$$Q_g = Q_{g,measurement} \pm \sqrt{\left(Q_g \cdot \delta^* Q_{g,specs,1} + \frac{150}{6 \cdot 10^4} \cdot \delta^* Q_{g,specs,2}\right)^2} \tag{2.37}$$

where (as pointed out in the section 'Equipment'), $\delta^* Q_{g,specs,1} = 0.5\%$ and $\delta^* Q_{g,specs,2} = 0.1\%$.

Similarly, for the liquid flow rate:

$$Q_l = Q_{l,measurement} \pm \sqrt{\left(Q_l \cdot \delta^* Q_{l,specs}\right)^2} \tag{2.38}$$

where $\delta^{*}Q_{l,specs} = 0.5\%$.

You can already imagine how the errors of the remaining measured quantities were accounted for. For calculated quantities, however, we needed to obtain the errors by taking into account propagation of uncertainty. For the mixing quantities x, we estimated the propagation of the error by saying:

$$\delta x_i = [\left(\frac{\partial x_i}{\partial \dot{m}_{ai}}\delta\dot{m}_{ai}\right)^2 + \left(\frac{\partial x_i}{\partial \dot{m}_{bi}}\delta\dot{m}_{bi}\right)^2 + \left(\frac{\partial x_i}{\partial \dot{m}_{ao}}\delta\dot{m}_{ao}\right)^2 + \left(\frac{\partial x_i}{\partial \dot{m}_{bi}}\delta\dot{m}_{bi}\right)^2 + \left(\frac{\partial x_i}{\partial C_{ai}}\delta C_{ai}\right)^2 + \left(\frac{\partial x_i}{\partial C_{bi}}\delta C_{bi}\right)^2 + \left(\frac{\partial x_i}{\partial C_{ao}}\delta C_{ao}\right)^2 + \left(\frac{\partial x_i}{\partial C_{bo}}\delta C_{bo}\right)^2]^{\frac{1}{2}} \tag{2.39}$$

I will only show the derivatives of x_1, as the rest will be similar in nature and can thus be reproduced in an alike fashion:

$$\frac{\partial x_1}{\partial \dot{m}_{ai}} = \frac{\dot{m}_{ao}(C_{ao} - C_{bi})}{\dot{m}_{ai}^2(C_{ai} - C_{bi})} \tag{2.40}$$

$$\frac{\partial x_1}{\partial \dot{m}_{bi}} = 0 \tag{2.41}$$

$$\frac{\partial x_1}{\partial \dot{m}_{ao}} = \frac{C_{bi} - C_{ao}}{\dot{m}_{ai}(C_{ai} - C_{bi})} \tag{2.42}$$

$$\frac{\partial x_1}{\partial \dot{m}_{bi}} = 0 \tag{2.43}$$

$$\frac{\partial x_1}{\partial C_{ai}} = \frac{\dot{m}_{ao}(C_{ao} - C_{bi})}{\dot{m}_{ai}(C_{ai} - C_{bi})} \tag{2.44}$$

$$\frac{\partial x_1}{\partial C_{bi}} = \frac{\dot{m}_{ao}(C_{ai} - C_{ao})}{\dot{m}_{ai}(C_{ai} - C_{bi})} \tag{2.45}$$

$$\frac{\partial x_1}{\partial C_{ao}} = -\frac{\dot{m}_{ao}}{\dot{m}_{ai}(C_{ai} - C_{bi})} \tag{2.46}$$

$$\frac{\partial x_1}{\partial C_{bo}} = 0 \tag{2.47}$$

As for the error terms $\delta(...)$, they are simply obtained using the manufacturer specified uncertainties mentioned in section 'equipment'. The mass flux (error) is related to the liquid flux (error) through

$$\dot{m} = \rho_l Q_l \tag{2.48}$$

The errors of the volumetric flux will also be estimated as given in Eq. 2.49.

$$\delta\beta = \frac{\partial\beta}{\partial Q_g}\delta Q_g + \frac{\partial\beta}{\partial Q_l}\delta Q_l \tag{2.49}$$

Chapter 3

Results

3.1 General

Before being able to explore mixing behavior across the two channels, we first needed to analyze the raw data, and decide whether we could continue using these for determining mixing values or not. That is why we will first show several key quantities measured, after which we will finally look at inter-channel mixing.

3.1.1 Velocities

As mentioned before, the original velocity files contained peaks of too high a value; values we could not use to e.g. calculate drift fluxes with. In Fig. 3.1(a) and 3.1(b), one can see peaks of over $80\,m/s$. The velocities have been plotted on a 48×48 grid, where each knot corresponds to a point on the same location of the wire-mesh sensor. The liquid flow rate of $81\,gpm$ corresponds with an Re_{DH} of $Re_{DH} = [4 \cdot 10^4 \quad 4 \cdot 10^4]$—the left and right value denote channel A and B respectively. After having adjusted the velocities using the method explained above, you will see a significantly more realistic portrayal of bubble velocities in Fig. 3.1(c) and 3.1(d). Maximum velocity peaks will not exceed $20\,m/s$, and a smoother surface is shown. A problem, however, occurs when, a peak is directly surrounded with more peaks. In that case, the scheme will use adjustment points that are too big in value, resulting in peaks still. Therefore, we repeated the smoothening process, until all velocities were below the set threshold. These data sets had been taken at a gap height of $20\,mm$. It would be too much showing figures of every single data set in this report; other data sets all showed images of very similar nature.

At higher gas flux, you clearly see an overall increase of the velocity throught the WMS. Note: Fig. 3.1(d)-location 'bi' is skewed (relatively) due to the colorbar handle maximum being higher, just as is the case in a few other figures here. A higher gas flux logically entails higher average velocities. At lower flux, you more readily notice an uneven distribution of the bubbles throughout the channel's cross-section, which appears to be most visible at the inlet locations. Furthermore, when comparing inlet and outlet distributions, you can also see that peaks from the inlet do not recur at the same positions at the outlets, indicating (random) movement of the bubbles throughout the cross-section. Still, we did notice a preference for the bubbles to stay at the walls of the channel (visually), which we also see in the WMS velocity distribution data. This was probably due to the injection needles being placed off-center, air flowing through the holes unevenly due to perhaps one hole being larger than the others. We simply 'accepted' this disparity in spatial distribution. Replacing the injection needles would take up too much of our time—we were subjected to major time constraints, as we already lost an entire month due to the optical probe problem. Having adjusted the velocities as a post-processing measure, this does not mean the problem has been solved. For the velocities unadjusted (i.e. those below the adjustment threshold), cross-correlation values were still much below a number as low as 0.5. As a matter of fact, a randomly taken data set showed that only 134 of the 2288 non-zero cross-correlation values (a little less than $48 \times 48 = 2304$) were (just) above 0.5. In the adjusted velocity data, we recognize values of over $2\,m/s$. A quick estimate would show these values to still be too high. See Eq. 3.1 for an estimate of the superficial gas velocity at 150 slpm ($= 0.0025\,m^3/s$) (see data table in the appendix for a summary of the data).

$$v_{g,sf} = \frac{Q_g}{\bar{\epsilon} A_{channel}} = \frac{0.0025}{11.24\% \cdot 0.0161} = 1.3\,m/s \tag{3.1}$$

whilst the superficial velocity of the gas was $v_{g,sf} = 2.4\,m/s$ at the highest gas flux (150 slpm) and highest liquid flux (201 gpm). This method is exactly the one we chose in order to obtain the velocity adjustment parameters (just rewritten), see *Methods*. For this, however, we assumed the WMS void fraction measurement to be accurate (otherwise there is no baseline for comparison). We did not observe any spurious void fraction data (see next subsection), so we did not find reason to believe data is incorrect, which is very 'unscientific', and quite frankly not allowed. The reason we still do, though, is because there have been various publications of researchers using the same HZDR-designed WMSs in their research, several after having done validation themselves [18] [19] [17]. We aimed to do that, but were not able to during my stay (optical probe problem), but will be done in the future. Interestingly, those authors have not used the WMs for velocity measurements; only void fractions and bubble size, which in our case will also be the only two quantities used.

In the future, when the WMSs have been put closer together in order to facilitate cross-correlation calculations, we expect the velocities to become more reliable for further studies.

3.1.2 Void fraction and bubble size

The void fractions plotted in time for a random data set of WMS at 'ao' have been displayed in Fig. 3.3. This particular data run operated on a gas flux of $Q_g = 50\,slpm$

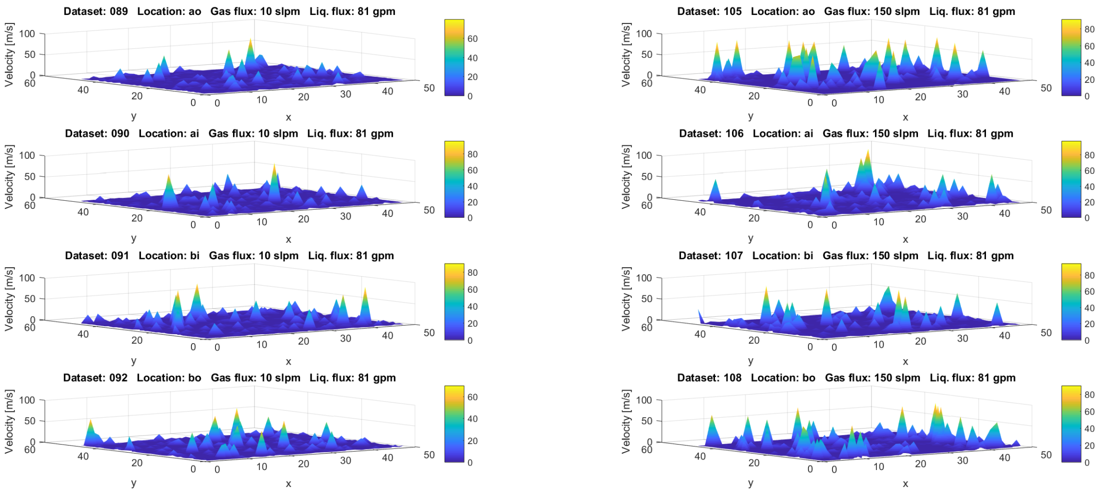

(a) Original; low gas flux ($Q_g = 10\,slpm$)

(b) Original high gas flux ($Q_g = 150\,slpm$)

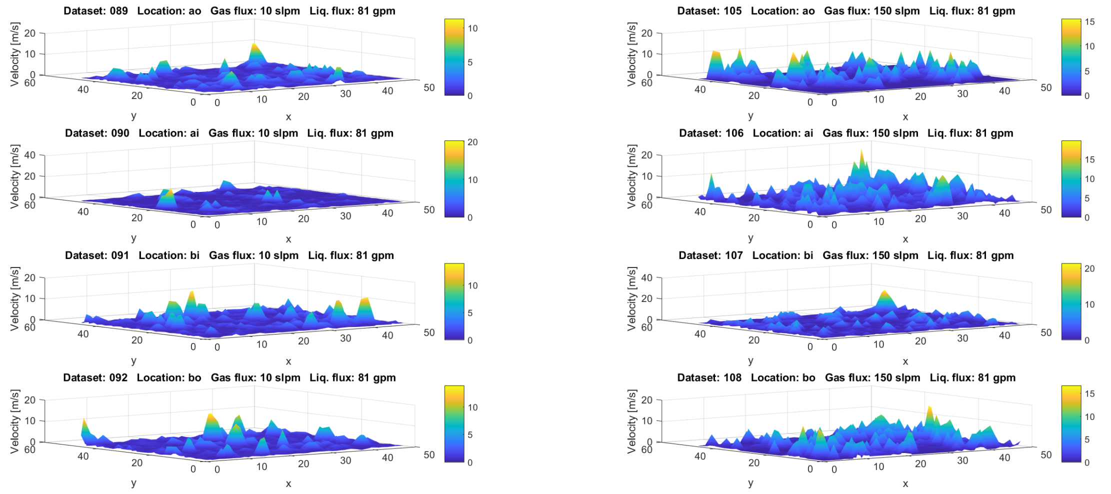

(c) Adjusted; low gas flux ($Q_g = 10\,slpm$)

(d) Adjusted; high gas flux ($Q_g = 150\,slpm$)

Figure 3.1: Velocity data for the $Q_l = 81\,gpm$ ($Re_{DH} = [4 \cdot 10^4 \quad 4 \cdot 10^4]$) case.

($= 8.3\,m^3/s$) and an Re_{DH} of $Re = [4 \cdot 10^4 \quad 4 \cdot 10^4]$, showing an average void fraction of $\bar{\varepsilon} = 9.0\%$ and a standard deviation of $\sigma = 1.1\%$. Only sensor 1 has been shown there. To reduce the amount of space used for figures, a void fraction summary of 21 various cases have been plotted in Fig. 3.4. As gas flux increases, void fraction logically follows to increase as well. We generally found sensor 1 to show higher void fractions than sensor 2. For the case displayed in Fig. 3.3, the average void fraction was $\bar{\varepsilon} = 8.3\%$ ($\sigma = 0.87\%$). Every time, sensor 2 showed a lower void fraction. This may probably be due to the sensor wires breaking up the bubbles into smaller ones. Also, as more smaller bubbles

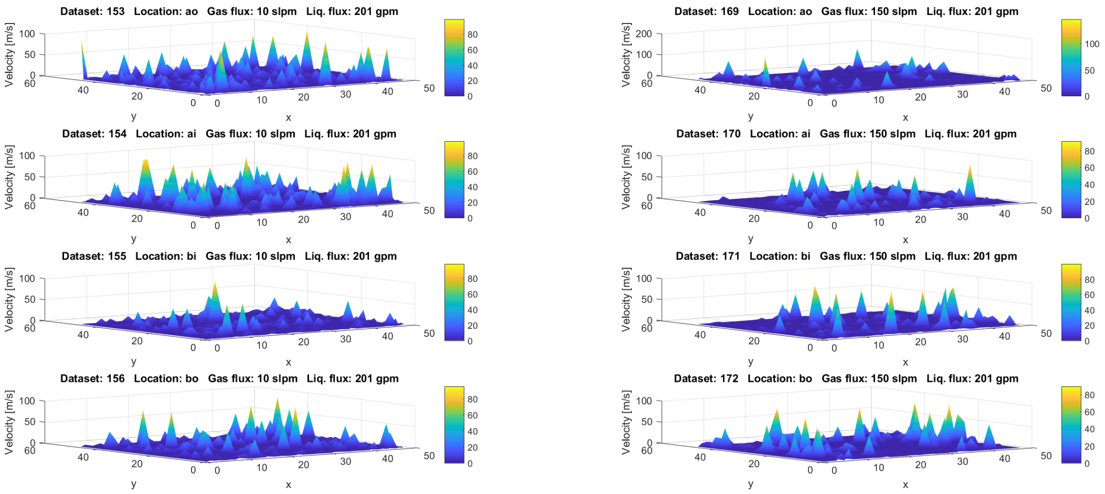

(a) Original; low gas flux ($Q_g = 10\,slpm$)

(b) Original high gas flux ($Q_g = 150\,slpm$)

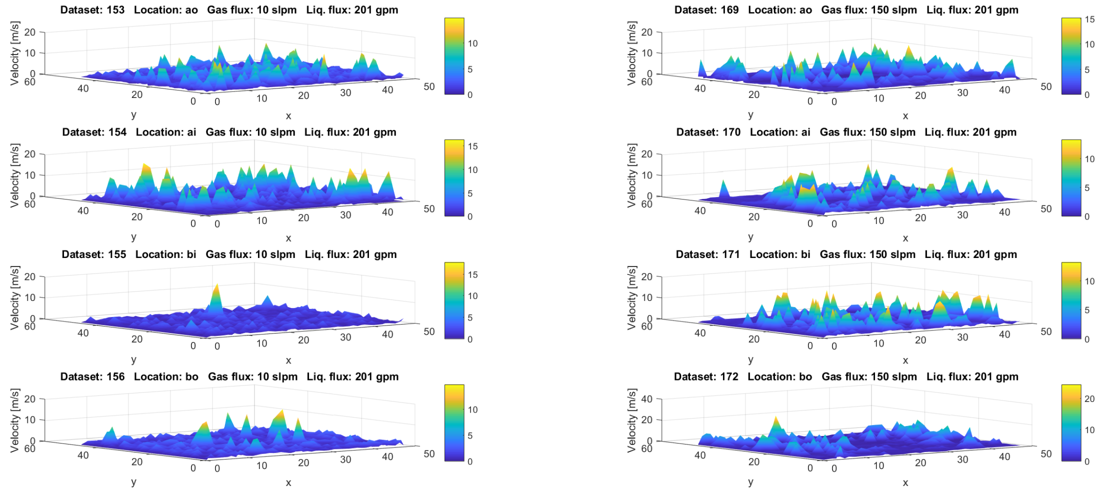

(c) Adjusted; low gas flux ($Q_g = 10\,slpm$)

(d) Adjusted; high gas flux ($Q_g = 150\,slpm$)

Figure 3.2: Velocity data for the $Q_l = 201\,gpm$ ($Re_{DH} = [1 \cdot 10^5 \quad 1 \cdot 10^5]$) case.

exist after passing through sensor 1, there will be a higher number of bubbles undetected by the second sensor. Furthermore, something worth noting is that for every single data run analyzed, outlet channel WMSs (ao, bo) displayed higher void fractions for the same gas flux put in. Over 50 data runs, an average void fraction growthof $\bar{\varepsilon}_{ao} - \bar{\varepsilon}_{ai} = 0.5\%$ is found, whereas for channel B this was f $\bar{\varepsilon}_{bo} - \bar{\varepsilon}_{bi} = 1.6\%$. This suggests that over the span of the column, bubbles coalesce to form large bubbles over an area, and thus increase void fraction. We did not find out the reason behind the difference in void fraction growth between the two channels, although we do suspect the difference in the thickness of the

WMS wires to affect this. We will further discuss this during the discussion. Still, whilst suggesting bubble coalescense to justify void fraction growth, bubble size measurements, however, show the opposite of what we would expect. The outlet channel bubble sizes appear to be higher every time: $\bar{d}_{ao} - \bar{d}_{ai} = -1.4\,mm$ and $\bar{d}_{bo} - \bar{d}_{bi} = -1.1\,mm$. The bubbles decrease in size throughout the channel length.

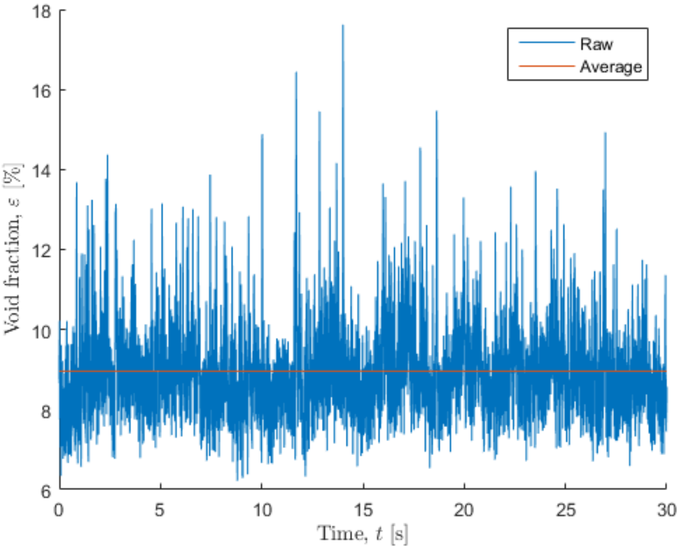

Figure 3.3: Void fraction measured in time for the case $Q_l = 81\,gpm$ ($Re_{DH} = [4 \cdot 10^4 \quad 4 \cdot 10^4]$)and $Q_g = 50\,slpm$ through channel ao.

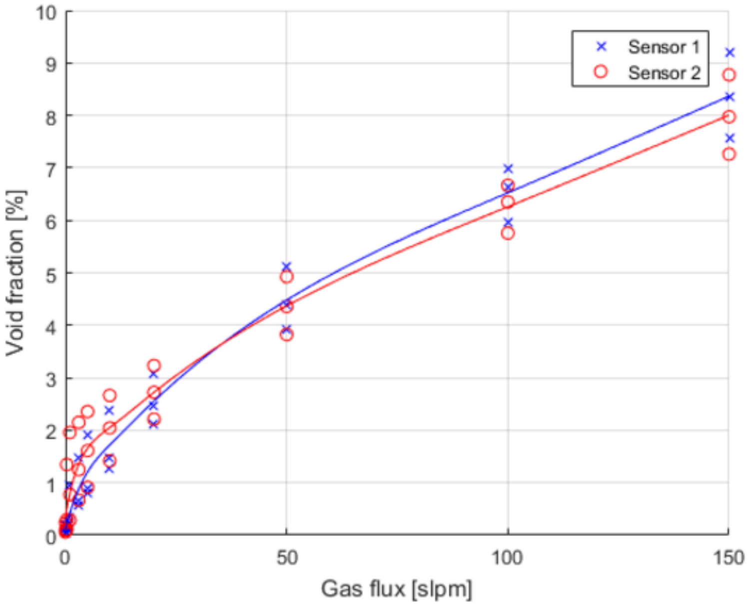

Figure 3.4: Gas flux plotted against for several liquid flow cases stacked ($Q_l = [121, 161, 201]\,gpm$) through channel ai.

To give you an idea on how the bubble size data we had looked like, see Figs. 3.5 and 3.6.

Low flux cases displayed 'clean' distributions, whilst noise became increasingly apparent with increasing gas flux. This was due to large bubbles coming into existence because of the sheer amount of bubbles being pumped into the channel, which we observed visually. The $9\,mm$-range did still contain the most bubbles. Also, the outlet WMSs showed to have more bubbles of the same size, compared to the inlet channel positions. Bubbles enter the channel just below the place at which the inlet WMSs have been placed, which would give the bubbles too little time for its size to reach a steady-state.

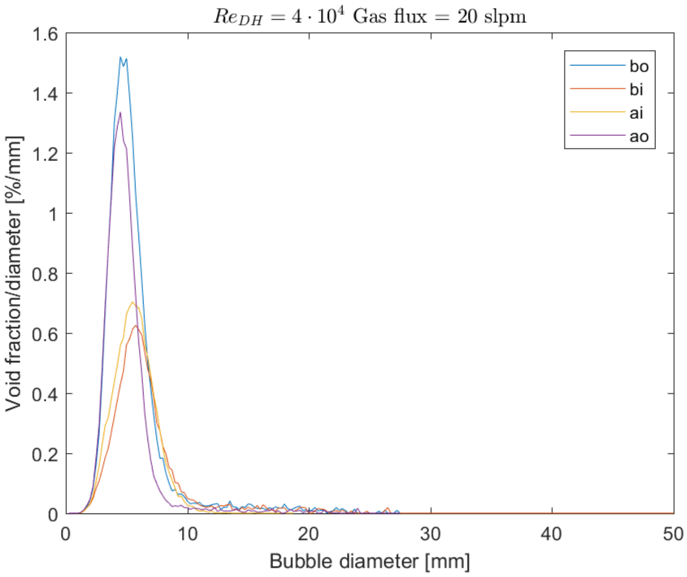

Figure 3.5: Bubble distribution for the case $Q_l = 81\,gpm (Re_{DH} = [4 \cdot 10^4 \quad 4 \cdot 10^4])$ and $Q_g = 20\,slpm$ for all four channels

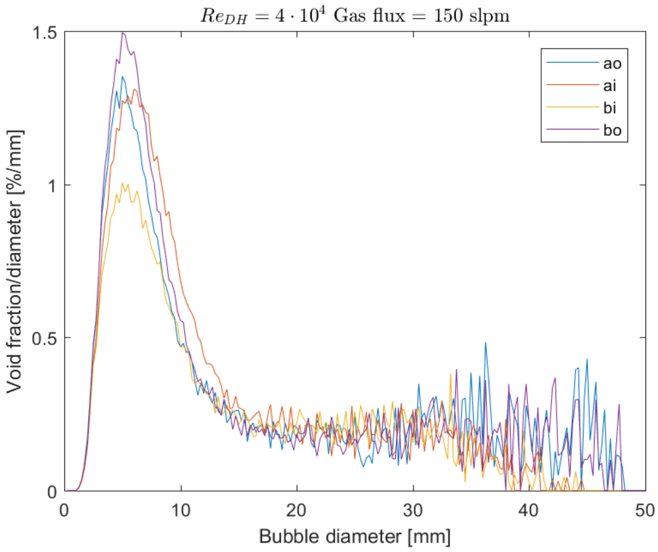

Figure 3.6: Bubble distribution for the case $Q_l = 81\,gpm$ $(Re_{DH} = [4 \cdot 10^4 \quad 4 \cdot 10^4])$and $Q_g = 150\,slpm$ for all four channels

As for the bubbles recorded using camera data, we generally found the diameters to not really coincide with the ones found using the WMs. This is especially so for high gas flux cases. The smallest gas flux is shown in Fig. 3.7 ($Q_g = 1\,slpm$), a flux so low, we did not even examine this case in our mixing research. The reason I embedded this here, is to give the reader a visually clear image of the bubbles processed. With higher gas fluxes, the image would be much too clogged with bubbles. Fig. 3.7 shows you the steps taken between raw and processed images. In the first step, the background is deleted from the picture, as the code removes all stationary objects and keeps those that are moving. Next (bottom-left), a binary colorscheme (100% contrast) image is made, in order for the bubble-searching program to distinguish the bubbles better. Finally (bottom-right), the code searches for kernels, looks for their outer edges, and calculates the diameter based on that. As you see, the camera unfortunately was not able to capture every bubble. Know that this is an image in the 'easiest' flow conditions for the camera to capture bubbles in. At gas flowing at $20\,slpm$, it already was impossible to properly identify the bubbles, because of their sheer amount. HSC data gave an average bubble size of $2.8\,mm$ upstream of the WMSs, and an average diameter of $1.2\,mm$ downstream of the WMSs. In Fig. 3.8, you see two diameter distributions: one before reaching the set of WMSs at channel ai, and one right after. It was impossible to film between sensors 1 and 2 because of the construction there being opaque (it was a metal wall).The figures clearly show a decrease in bubble size as they move through the WMSs. You can also see that these bubbles vary more in size before they get 'split' into ones of more equal size.

Finally, for an overview of the mean bubble diameters, see Tab. 3.1.

Table 3.1: Average area-equivalent bubble diameters for different volumetric gas flowrates and Reynolds numbers, measured using the outlet WMSs

Q_g $[m^3s^{-1}]$	Re $[-]$			
	$4 \cdot 10^4$	$6 \cdot 10^4$	$8 \cdot 10^4$	$1 \cdot 10^5$
0	0	0	0	0
$2.0 \cdot 10^{-4}$	5.1	4.5	4.6	4.3
$4.0 \cdot 10^{-4}$	5.6	5.8	5.1	4.8
$1.0 \cdot 10^{-3}$	7.1	5.5	5.5	5.2
$2.0 \cdot 10^{-3}$	10.8	9.5	10.5	9.1
$3.0 \cdot 10^{-3}$	15.4	11.9	13.2	13.0

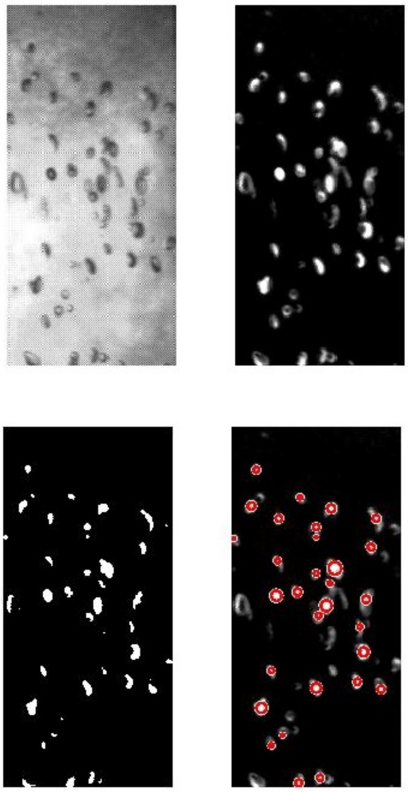

Figure 3.7: Camera bubble data for $Q_l = 81\,gpm$ ($Re_{DH} = [4\cdot 10^4, 4\cdot 10^4]$) and $Q_g = 1\,slpm$

3.2 Mixing

3.2.1 C7 data

See Fig. 3.9 for dye concentration data measured throughout a data run. As a valve that connects a channel position with the dye sensor is opened, you see a certain dye concentration being measured. Valve 3, which is *ai*, is turned on first (after the the flush), and does not lead to any significant dye measurements, as *ai* is the point *before* the gap, where only fresh water enters. Measuring dye there, would mean the wave tank has been contaminated with dye too much. As a matter of fact, as already mentioned before, before commencing any data run, we made sure the concentrations of dye in the water flowing through the channels were low enough. Next, you see valves 4, 5, and 7 opening subsequently. As they are all located at *ao*, the same concentrations of dye are measured. For this specific case, these concentrations are $C_{ao} \approx 2.56\,ppb$. Despite dye coming in from channel B (valve 10 is *bi*; valve 9 is *bo*) through the gap—read: despite 'mixing'—these concentrations are still quite low. You will see later on that this is due to the gas flux being as high as it is at $100\,slpm$, and because the gap height is only $20\,mm$. Furthermore, you may notice the red line being just outside the interval during which the valve is opened. This is because of valuable information regarding the dye concentration of

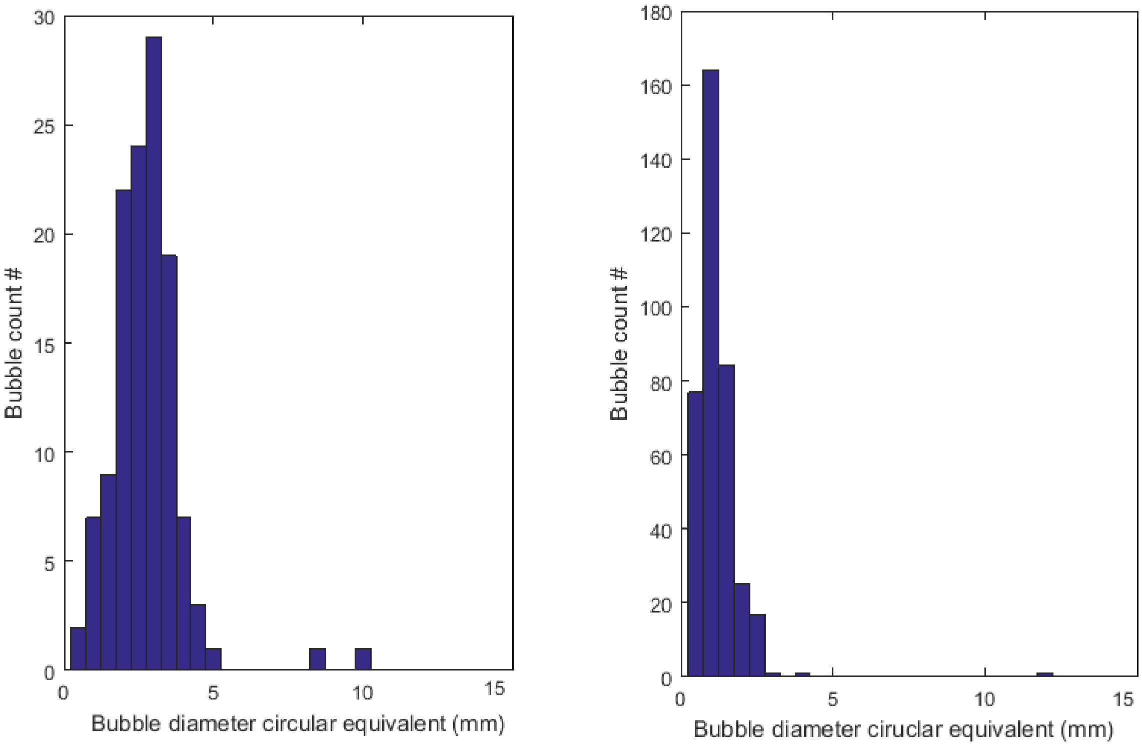

(a) Upstream (before the first WMS)

(b) Downstream (after two WMSs)

Figure 3.8: Camera bubble data for $Q_l = 81\,gpm$ ($Re_{DH} = [4 \cdot 10^4 \quad 4 \cdot 10^4]$) and $Q_g = 1\,slpm$ at channel ai, taken at 30 FPS

a channel does not subside until some time later on, and we did not intend to dismiss that, especially since the first half (approximately) is being disregarded to ensure a steady-state dye level. In this particular case, the *bo* concentration was $C_{bo} \approx 180\,ppb$, and at the inlet the concentration was $C_{bi} \approx 191\,ppb$.

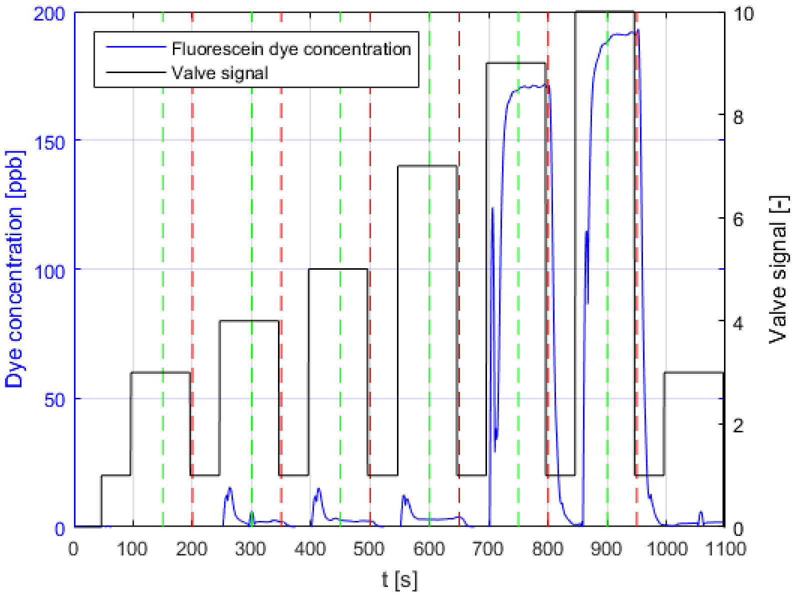

Figure 3.9: C7-signal data. The dashed vertical lines delineate the area of data points that are being used to calculate mixing coefficients. The green ones denotes the start, the red ones the end of the interval. This data set has been taken at $Q_l = 81\,gpm$ ($Re_{DH} = [4 \cdot 10^4 \quad 4 \cdot 10^4]$), $Q_g = 10\,slpm$, and a gap height of $50\,mm$.

I find it personally valuable to not put forth a skewed representation of reality here. Fig. 3.9 is an almost ideal case to have, whilst there have been many data sets with completely unsteady signals, rendering them unfit for any usage at all. Look at Fig. 3.10, for example. This figure is one that is *just* about useable. The figure shows larger peaks, and there seems to be just enough time for the flushing to remove all dye residue: just as the concentration hits $\sim 0\,ppb$, another valve opens. Without flushing, we would not with certainty know how much residual dye would affect the measured concentrations. Increasing measurement times was also not that good of a possibility, because of the aforementioned dye recirculation issue (see *Methods*). Also notice that because of recirculation the total measurement time for the $Re_{DH} = [1 \cdot 10^5, 1 \cdot 10^5]$ case had to be reduced significantly.

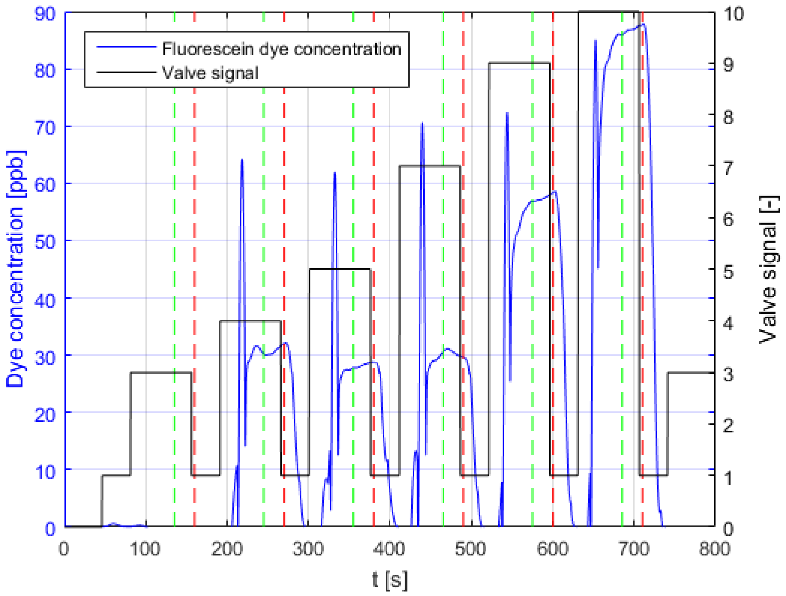

Figure 3.10: C7-signal data taken at $Q_l = 201\,gpm$ ($Re_{DH} = [1 \cdot 10^5, 1 \cdot 10^5]$), $Q_g = 0\,slpm$, and a gap height of $50\,mm$.

3.2.2 Mixing coefficients

Gap height: $50\,mm$

After having made sure our C7-signal data was actually useable the mixing coefficients, $\bar{x}$ and $\bar{y}$, have been obtained. Know that $\bar{x} = 0$ indicates zero mixing from side A to B, whilst $\bar{x} = 1$ means that outlet channel A, ao, attained the the same level fluorscein concentration as inlet channel B had. Mixing coefficient $\bar{y}$ is the exact opposite, as it denotes mixing from side B to side A.

See Fig. 3.11 for the mixing data plotted against six different gas fluxes (0, 10, 20, 50, 100 and 150 $slpm$) and four different Reynolds numbers ($40K$, $60K$, $80K$ and $100K$) for the $50\,mm$ gap height case. These Reynolds numbers correspond to liquid water flowrates of $5.0 \cdot 10^{-3}$, $7.6 \cdot 10^{-3}$, $1.0 \cdot 10^{-2}$, and $1.2 \cdot 10^{-2}$ $m^3 s^{-1}$ (or 81, 121, 161, and $201\,gpm$. Fig. 3.11(a) contains one extra volumetric flow rate: $Q_g = 5\,slpm$. You may notice a difference other than a factor $\frac{1}{6 \cdot 10^4}$, when converting to SI-units. The extra difference is due to a pressure correction we applied to the flow rate value: $Q_g = Q_{gFM}\left(\frac{p}{p_{atm}}\right)$—for a vertical channel, the volumetric flowrate of gas requires a correction based on the local pressure p with respect to the pressure at the corresponding flow meter location (p_{FM}) in order to account for compressibility. The reason we added another flowrate will be discussed later on.

First, we need to mention the fact that at the zero flux case ($Q_g = 0\,slpm$) the mixing coefficients are both approximately $\bar{x} \approx \bar{y} \approx 0.33$, irrespective of the experiment's Reynolds number. Equal mass transfer from channel A to B and B to A is expected as the flow speed, geometry of both channels are nominally identical, and thus there is no mean spanwise pressure difference across the gap. As mentioned in the beginning, large-scale vortices forming at the channel gap interface occurred at a nominally constant Strouhal number (approx. 0.24 to 0.25)—see Fig. 3.12 for a visual— which suggests that leakage through a narrow gap should be independent of Re_{DH} (over the parameter range studied) for a specified gap height. Furthermore, equal mixing between the two channels coupled with visual observation of temporally stable vortex shedding downstream of the gap opening indicated that the Kelvin-Helmholtz type instability causing the large vortical structures is the dominant source of mixing between the two vertical channels. This instability occurs when there is a velocity difference across interfaces of two fluids; in our case between the high-velocity channel inlet, and the low-velocity gap region.

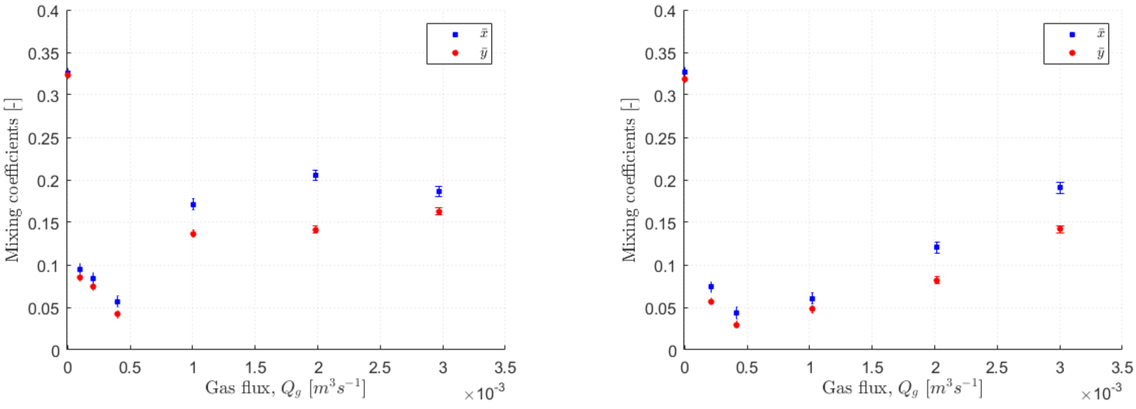

(a) $Re = [4 \cdot 10^4, 4 \cdot 10^4]$

(b) $Re = [6 \cdot 10^4, 6 \cdot 10^4]$

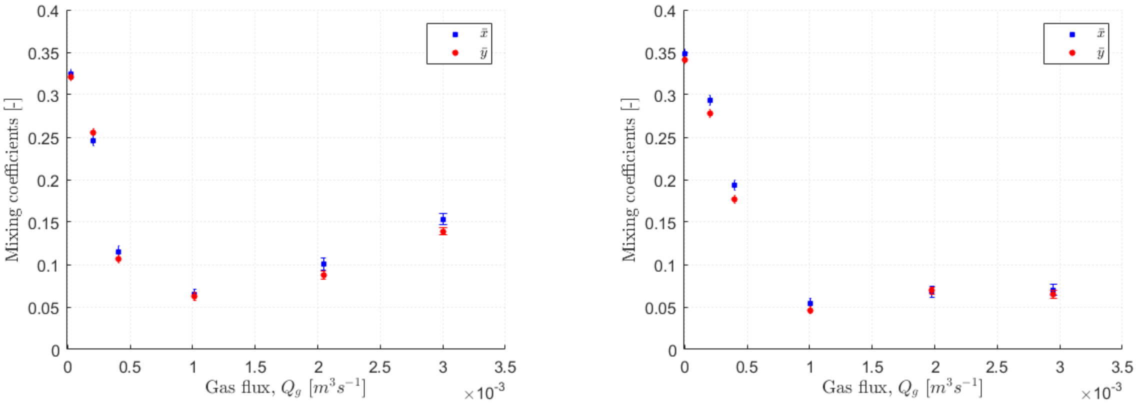

(c) $Re = [8 \cdot 10^4, 8 \cdot 10^4]$

(d) $Re = [1 \cdot 10^5, 1 \cdot 10^5]$

Figure 3.11: The mean mixing coefficients $\bar{x}$ and $\bar{y}$ plotted against the gas flux at different Reynolds numbers for the 50 mm gap height case.

The large vortices that shed in the gap for the single-phase flow case are significantly altered and obstructed from properly existing as air bubbles are injected into the system.

Injecting even a minimal volume of gas significantly inhibited mixing between channels A and B, as seen from Fig. 3.11. We included an even smaller amount of gas in the first Reynolds case, Fig. 3.11(a), which was $Q_g = 5\,slpm$ ($\approx 0.1 \cdot 10^{-3} m^3 s^{-1}$), to see whether this large of an inhibition in mixing would be present with such a small amount of gas as well. Judging from the results, it still was. By simply defining an inhibitation number as the difference of the mixing coefficients with and without gas flux, normalized the single-phase mixing coefficient, i.e. $I_{n,x} = \frac{x_0 - x}{x_0} = 1 - \frac{x}{x_0}$, we can quantify how the mixing is inhibited for the cases of bubbly channel flow as compared to the single-phase case. $I_{n,y}$ would then define the inhibition number when looking at the y-coefficient of mixing. At low Re_{DH}, the mixing coefficients x and y were significantly reduced at even the smallest gas fluxes. At the $10\,slpm$ region, the mixing coefficients were nominally equal at 0.08, yielding an inhibition number as high as 0.75. Further increasing the gas flux to $20\,slpm$ ($Q_g \approx 0.4 \cdot 10^{-3}\, m^3 s^{-1}$) further inhibts mixing at these low-Re_{DH} flows, resulting in an inhibtion number of 0.85. At this flux a local minimum appears to have been reached, which is the case for the two lower Re_{DH} numbers.

After this minimum, increasing the volumetric gas flow rate means increasing mixing. However, I_n never reaches a value smaller than 0.40, which is the inhibition number at the highest mixing rate for the multi-phase flow regimes tested: at $x \approx y \approx 0.20$—I am talking about the low-Re_{DH} cases. There also seems to be a very significant disparity between the x and y mixing coefficients at the higher flux regions at these low Re_{DH}. In the *Discussion* section, an attempt will be done in explaining these observations. Mixing inhibition is present for all Re_{DH} tested, however the volumetric gas flowrate at which its maximum (i.e. minimum mixing) appears, does shift to the right for higher Re_{DH} cases: at $Q_g \approx 1 \cdot 10^{-3}\, m^3 s^{-1}$. Furthermore, mixing seems to be a lot less low for low-end gas fluxes at higher Re_{DH}. Furthermore, increasing the gas flux at high Re_{DH} seems to influence mixing a lot less, compared to lower Re_{DH} cases. Also, reduction in mixing can be visually observed, see Fig. 3.12(b), as you may notice the large-scale structures being disrupted due to the presence of the injected air bubbles. The distinctly moving cloud of fluorscein dye mixture has turned into an unstable two-phase flow mixture, resembling a Rayleigh-Taylor type instability, which is an instability that occurs between the interfaces of fluids of different densities (water and air in our case), where the lighter fluid (air bubbles) is pushing the heavier fluid (water).

Gap height: $20\,mm$

Next to the $50\,mm$ gap height case, another gap height had been set for analysis as well. For their mixing values plotted against the volumetric gas flowrate similar to what you have seen before, see Fig. 3.13. The $20\,mm$ gap cases showed inconsistent zero-flux mixing values, contrary to the $50\,mm$ gap height case, as these values kept varying within the 0.1 and 0.15 limits. At $Re_{DH} = [4 \cdot 10^4, 4 \cdot 10^4]$, at even the zero-flux case a difference in x- and y-mixing was present. These differences became even more so present at $Q_g = 2 \cdot 10^-3\, m^3 s^{-1}$ ($\approx 100\,slpm$), which also showed to be the highest mixing disparity case at the previous gap height. Also similar to the previous case, high Reynolds number

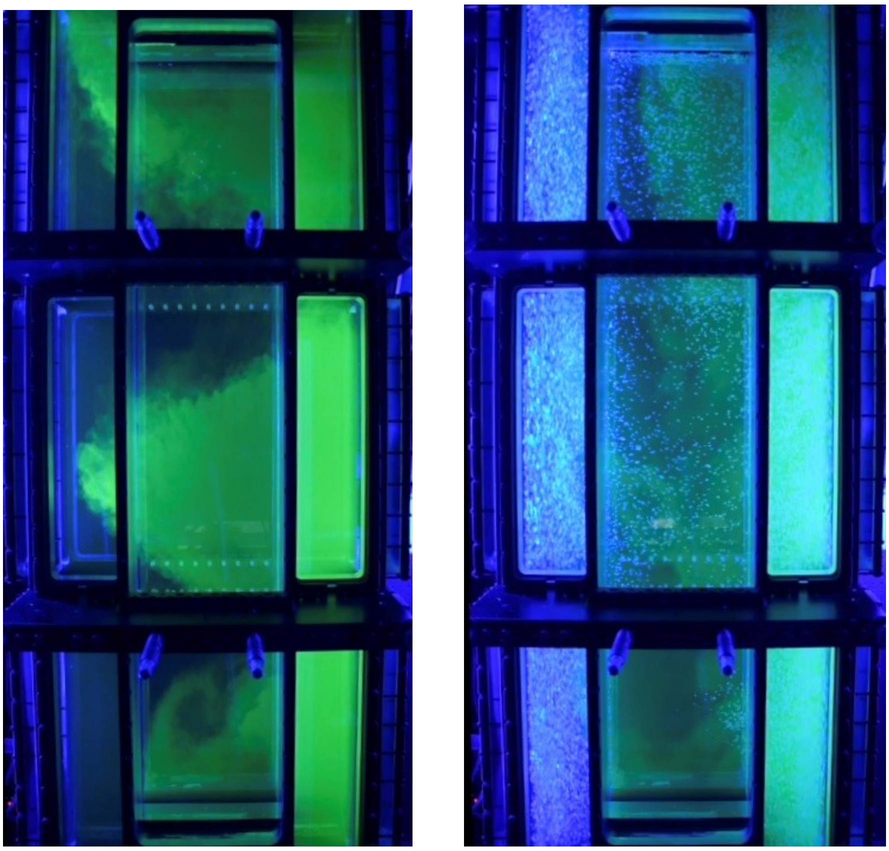

(a) Single-phase flow: $Q_g = 0\,slpm$ case

(b) Multi-phase flow: $Q_g = 20\,slpm$ case; $\bar{\varepsilon} = 4\%$.

Figure 3.12: Camera footage of mixing cases at $Re = [6 \cdot 10^4, 6 \cdot 10^4]$ at a gap height of $50\,mm$. Green fluorescein dye injected upstream of the gap in channel B (right channel) provides visual evidence of the large, coherent flow structures, which dominate the liquid mass transfer between the two channels, through the narrow gap for the single-phase flow in 3.12(a). The coherent structures are drastically suppressed with the presence of the air bubbles, as shown in 3.12(b).

flows did not show that much significant disparity in mixing at all. Apparently, this phenomenon only seems to emerge at lower liquid flowrates.

In general, mixing coefficients are significantly lower due to the smaller gap. Where the single-phase case at $50\,mm$ showed a mixing rate of $x \approx y \approx 0.33$, the $20\,mm$ case showed values less than half of that: $x \approx y \approx 0.13$.The largest inhibiton factor $I_{n,x}$ at the $Re_{DH} = [4 \cdot 10^4 \quad 4 \cdot 10^4]$ case is $I_{n,x} = 0.76$, which is a little less than $I_{n,x} = 0.83$ at the larger gap height. Most inhibition factors are around 0.75 for the $20\,mm$ case. We observe that at increasing gas flux, mixing rates do not increase as much as they did at the previous gap height. The lowest Reynolds number case did show mixing to increase at increasing gas flux after having passed minimum mixing. As for the positions at which minimum mixing takes place, these occur at the $\approx 20\,slpm$ gas flowrate for the lower Reynolds numbers, and ≈ 50 *slpm* for $Re_{DH} = [8 \cdot 10^4 \quad 8 \cdot 10^4]$, and as much as ≈ 100 *slpm* for the highest Reynolds number. A stretching behavior is observed, just like observed at the larger gap height. Also, looking at the highest Reynolds number, the 10 *slpm* case did not seem to inhibit mixing as it did with every single other 10 *slpm* case previously examined, which made us doubt the validity of the data gathered for this specific case. Furthermore, while the 20 *mm* gap height case shows most mixing coefficients to be equal to or below the value of 0.05, the 50 *mm* gap case only had three of those cases: the three minima at $Re_{DH} = 4 \cdot 10^4$, $Re_{DH} = 6 \cdot 10^4$, and $Re_{DH} = 1 \cdot 10^5$.

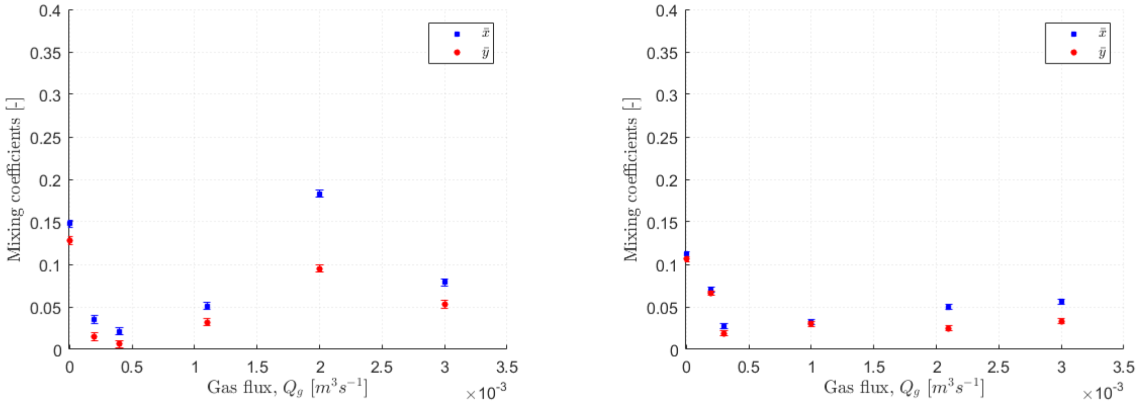

(a) $Re = [4 \cdot 10^4, 4 \cdot 10^4]$ (b) $Re = [6 \cdot 10^4, 6 \cdot 10^4]$

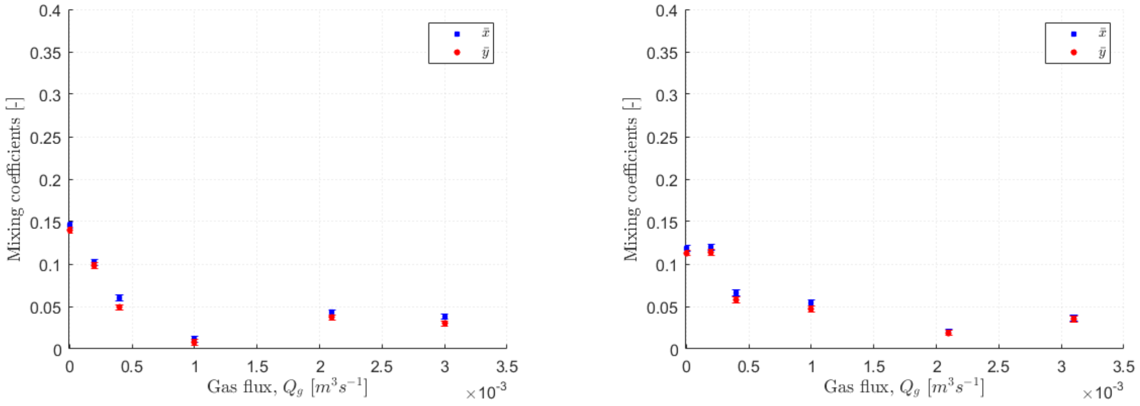

(c) $Re = [8 \cdot 10^4, 8 \cdot 10^4]$ (d) $Re = [1 \cdot 10^5, 1 \cdot 10^5]$

Figure 3.13: The mean mixing coefficients $\bar{x}$ and $\bar{y}$ plotted against the gas flux at different Reynolds numbers for the 20 *mm* gap height case.

Chapter 4

Discussion

In this section, we will try to go more in-depth with the results presented in the previous chapter. An attempt will be made to look for similarity in mixing between the different Reynold number cases and gap heights. Also, we will try to see whether the mixing coefficient discrepancy can be explained (is it 'real' in the first place?), which will end with some suggestions concerning future studies.

4.1 Mixing

4.1.1 General observations

We could make the x-axis of the previously shown mixing figures (annotated with the gas flow rate Q_g), dimensionless by using the volumetric quality β instead (see Eq. 2.32). The mixing coefficients plotted now, will be the average mixing coefficients $\bar{X} = \frac{1}{2}(\bar{x} + \bar{y})$. Note that the volumetric quality can only ever run between $\beta = 0$ and $\beta 1$, as $\beta 0$ would denote the single-phase case, and $\beta = 1$ the case in which $Q_g \to \infty$.

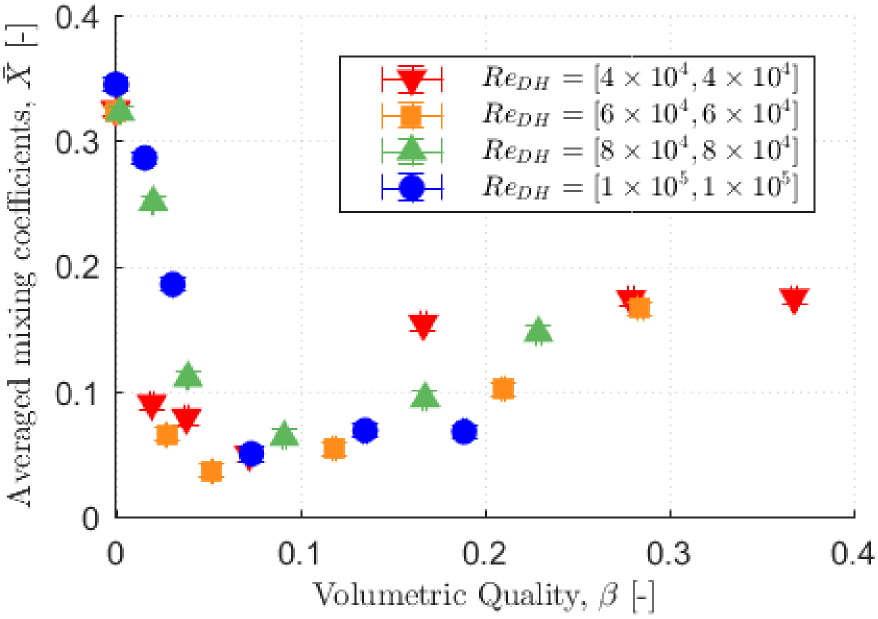

Figure 4.1: Average mixing coefficients were shown to vary with the volumetric quality of the inlet mixture at a gap height of 50 mm. The results are insensitive to changes in the channel Reynolds number.

Looking at Fig. 4.1, you see that most of the data collapses at the different Reynold numbers, although for the 20 mm gap case this is somewhat less so (see Fig. 4.2). These figures demonstrate that integral mixing depends on the volumetric ratio of gas to the total two-phase flux. The average mixing coefficient at $\beta = 0$ seems to drop steeply with increasing volumetric quality, which increases again after having 'dipped' at around $\beta \approx 0.06$. Then, after a gradual rise, the mixing rate plateaus at $\bar{X} \approx 0.18$. You see that the lower Reynolds numbers cover the higher end of the volumetric qualities more, and the higher Reynolds numbers the lower end. The reason for this local minimum is not entirely clear. Inhibition of mixing because of the added bubbles, may be due to these these bubbles being a physical obstruction for the liquid to pass from one side, through the gap, to the other. Also, because the bubbles' velocities are larger than the liquid velocities (buoyancy), the velocity vectors of the liquid particles will have a larger z-component (axial direction), which makes it less likely for the liquid to mix. Most importantly, however, is the fact that the bubbles break the large alternating vortex structures that are being shed at the gap start. These large scale structures visually showed to be the key components of integral mixing.

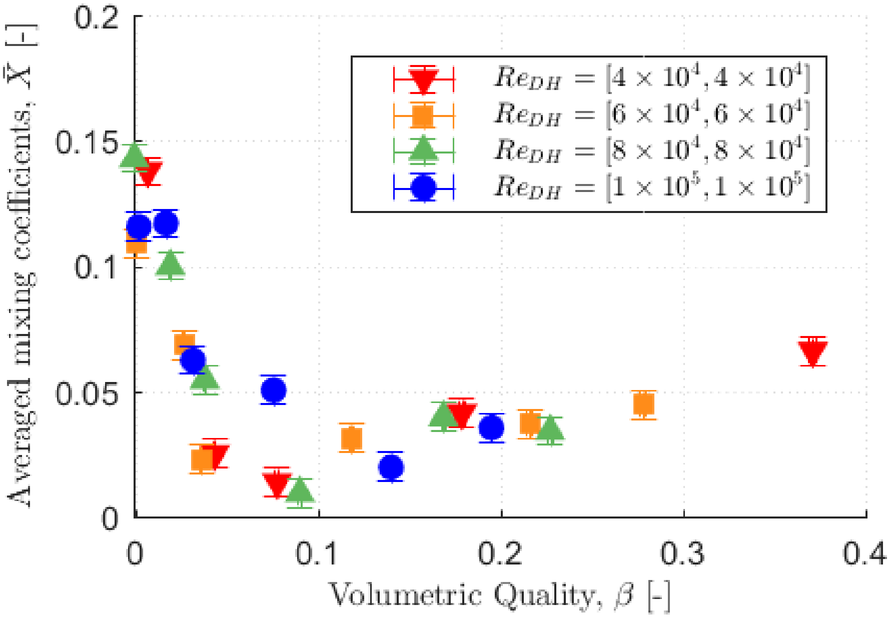

Figure 4.2: Average mixing coefficients were shown to vary with the volumetric quality of the inlet mixture at a gap height of $20\,mm$. The results are insensitive to changes in the channel Reynolds number.

As for the smaller gap case, we found that the single-phase case showed mixing coefficients of around 0.13 on average, which is consistent with what we found for previous studes [7]. However, Fig. 4.2 shows two cases to be just above, and two just below these previously found mixing coefficients, so we may be dealing with experimental errors here. What Fig. 4.2 does show, what is harder to notice in the dimensional figures, is that with increasing gas flux, the mixing coefficients actually do show an increase in value, although this observation entirely depends on the validity of the data at $Re_{DH} = [4 \cdot 10^4, 4 \cdot 10^4]$ and $Q_g = 150\,slpm$ (i.e. the right-most red upside-down triangle at almost $\beta = 0.4$). The $10\,slpm$ case for $Re_{DH} = [1 \cdot 10^5, 1 \cdot 10^5]$ (i.e. the $\beta \approx 0.02$ case) had a higher value than the zero-flux case, which contradicts every observation at that gas flowrate we have had before. Although the fluorescein data does not show to have any peculiarities, we suggest to redo that data set.

Two-dimensional collapsing of data

As we have noticed the data to stack for different Reynolds numbers, showing mixing to be invariant from the Reynolds number when plotted against the volumetric quality, we tried looking for ways to find similarity in mixing for different gap heights. We simply introduced a dimensionless length scale, H/H_0, and defined a new mixing coefficient:

$$\tilde{X} = \left(\frac{H}{H_0}\right)\bar{X} \tag{4.1}$$

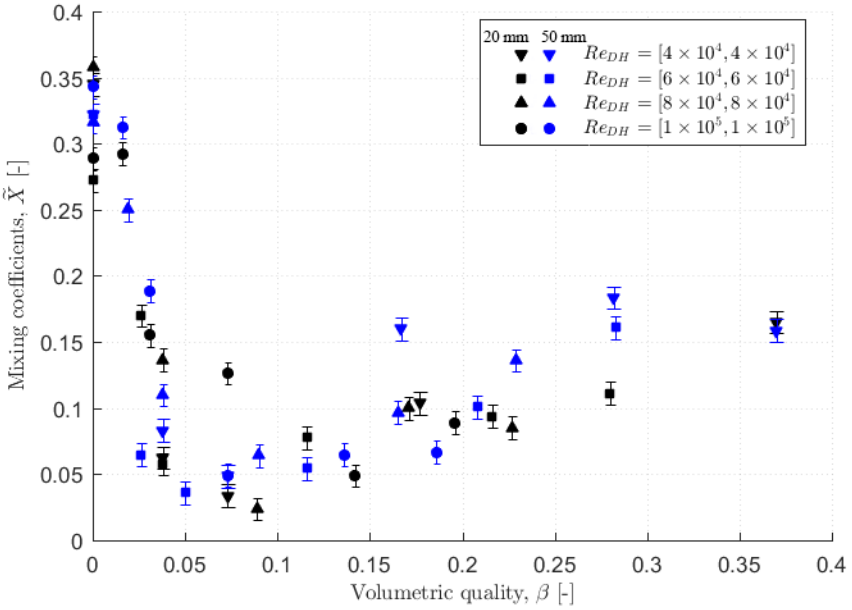

Figure 4.3: Adjusted mixing coefficient $\tilde{X}$ that incorporates the gap height plotted against the volumetric quality β

Fig. 4.3 shows that the new average mixing coefficients $\tilde{X}$ vary with the volumetric quality of the inlet mixture, independent of both the Reynolds number and the gap height. The data stacks on top of the 50 mm gap height data, as we set the reference gap height H_0 to be $H_0 = 50 \cdot 10^{-3}$. At the zero-flux case one still notices some significant differences in the mixing coefficient, just like we observed earlier, which means there is certainly still some room for improvement; naturally, this goes for other cases as well.

What about the inhibition number? Does mixing inhibition happen to be independent of gap height? Just like in the previous case, it is difficult to decide upon that with only two gap heights investigated, but it remains interesting nevertheless. Let us take a look at the four plots in Fig. 4.4. The inhibition numbers do show to fairly match, especially the low-flux cases (the case at which $I_{nx} < 0$ for $Re_{DH} = 4 \cdot 10^4$ is probably incorrect). It is interesting that this method of visualizing data shows somewhat of a stack between the gap heights, yet do not do anything to incorporate a dimensionless parameter which involves the gap height. Does this mean that we can characterize mixing inhibition for each gap height using just the volumetric quality?

Let us see what this stacking would actually look like in Fig. 4.5. It may surprise you that the data stack that nicely, but when looking back at Fig. 4.4, you may notice that the x-axes did not coincide, giving you a distorted 'relative' image of reality. The plot looks like the inverted form of the previous figures (Fig. 4.1 and Fig. 4.2), yet incorporates both in one figure now. Furthermore, the difference between Fig. 4.3 and this one (Fig. 4.5), is that the former uses a length scale to get the mixing data stacked, whilst the latter does not. The inhibition seems to increase with increasing volumetric quality, up until $\beta \approx 0.073$, where a maximum inhibition of $I_{n,x} \approx 0.85$ is reached. After that, inhibition

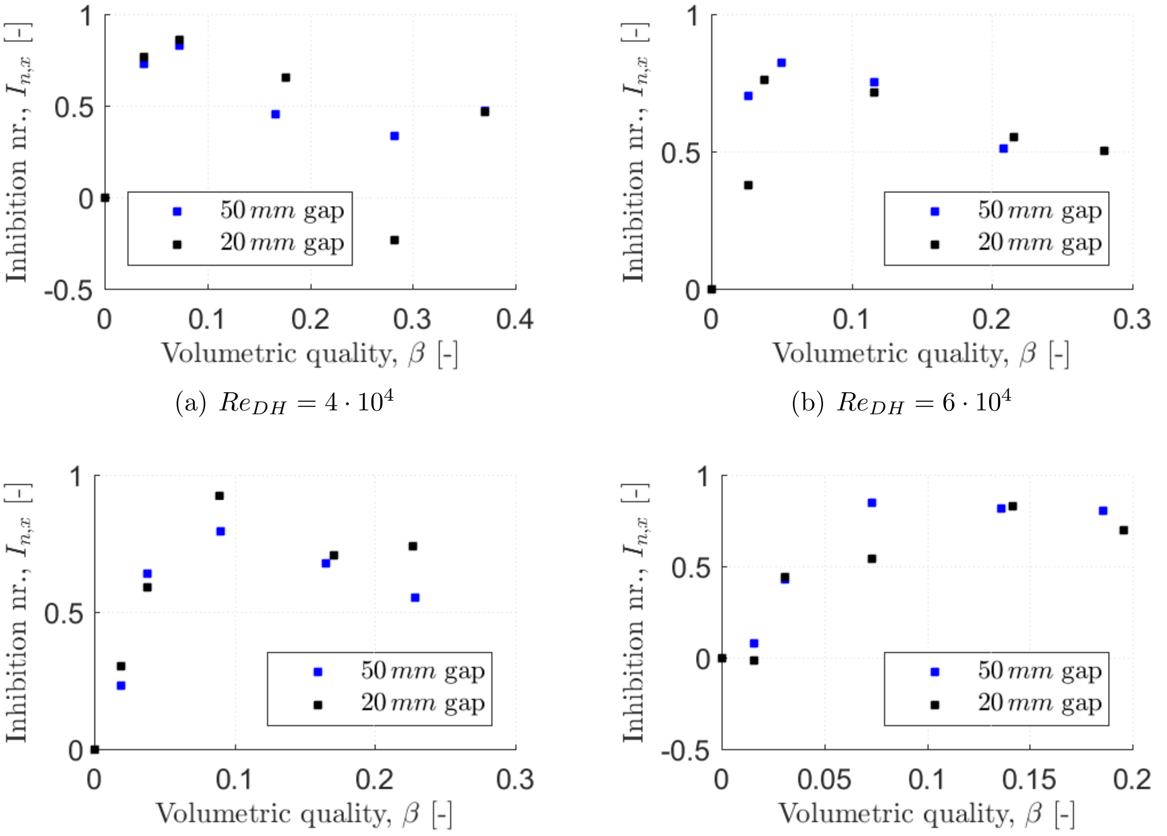

(a) $Re_{DH} = 4 \cdot 10^4$

(b) $Re_{DH} = 6 \cdot 10^4$

(c) $Re_{DH} = 8 \cdot 10^4$

(d) $Re_{DH} = 1 \cdot 10^5$

Figure 4.4: Inhibition numbers for x plotted against the volumetric qualities for different Reynolds number cases.

slowly decreases with increasing volumetric quality. When using this particular geometry set-up, one may refer back to the mixing coefficients through the inhibition number at a given β, as long as the single-phase mixing values for the case one wants to study are known:

$$x(I_{n,x}(\beta)) = x_0\,(1 - I_{n,x}(\beta)) \tag{4.2}$$

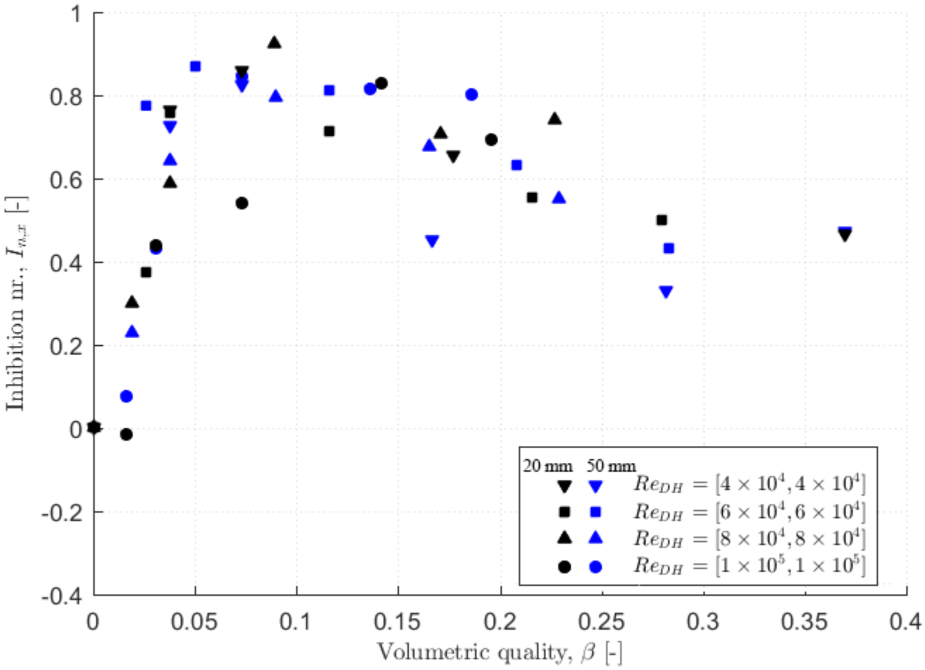

Figure 4.5: The inhibition numbers for x plotted against the volumetric qualities for all Reynolds numbers investigated.

4.1.2 Fluorescein data problems

As for the experimental errors, we already noticed that when we discovered the large mixing disparities at some points in our data sets. Also, the very low mixing values (the ones almost approaching zero-mixing in the Fig. 4.2 or in the Figs. given in *Results*) may like be not as correct as we want or expected them to be, for when further examining the fluorescein data, considerable unsteady was found to exist. See Fig. 4.6. Several comments may be made regarding these data. The *bo* part of the fluorescein data signal (i.e. when valve signal equals 9) seems to be unsteady in that it is constantly rising in dye concentration, until the sensor simply stopped measuring. As no steady-state concentration had been reached, we cannot say that the average of this rising trend is correct. Furthermore, when zooming in at the *ao* measurements—see Fig. 4.6(b)—you see a similar rather unsteady behavior in the data. Whilst valve 5 (the middle one) seems somewhat steady, the other ones are clearly not. On top of that, flushing only barely seemed to work as the line only barely touched the zero-concentration point.

Another data set that showed undesirable fluorescein results was the one shown in Fig. 4.7. The problem in this data set is the large amount of peaks found at the *ao* measurement location, which naturally affects the dye concentration average measured. A likely cause of these peaks may be imperfect separation of phases just before the C7-sensor. As water mixed with bubbles enter the tubes that lead to the C7-sensor, all liquid and gas must be separated, lest one wants to assure a constant measurement of dye. Whenever a bubble

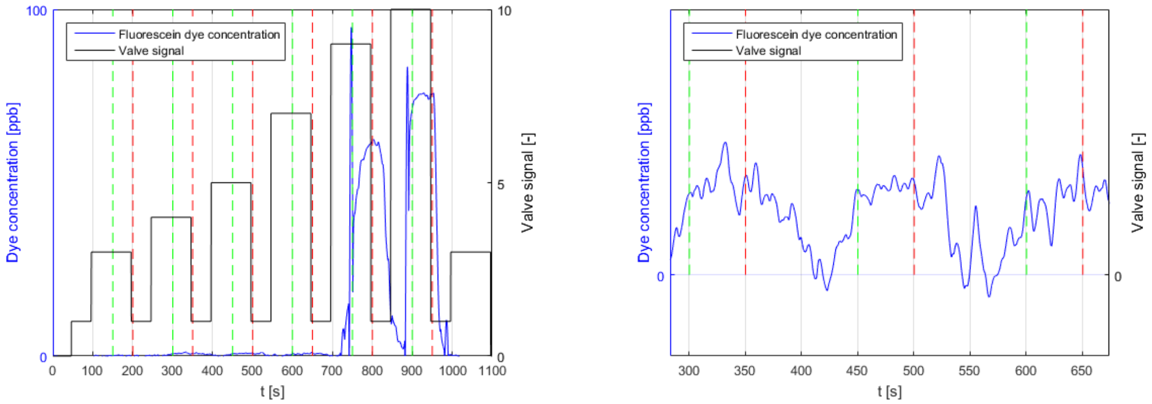

(a) Total. (b) Zoomed in at the *ao* measurements.

Figure 4.6: Fluorescein data for the $20\,mm$ gap case at $Re_{DH} = [8 \cdot 10^4, 8 \cdot 10^4]$ and $Q_g = 100\,slpm$.

gets trapped, the sensor briefly measures 'nothing', after which it measures 'something' again. These very sudden changes in measurements usually lead to some overshoot in the afterwards steady signal. This naturally happens at the beginning of each valve opening, as you can see from the figures. We ignored these peaks by simply only looking at the values that come after. When these peaks occur too often, however, those values get distorted as well and may thus render an entire data set unusable. An option is that one could just filter out these peaks during post-processing.

As far as improper phase separation is concerned, one can actually see this happening if one pays attention during the experiment. The difficulty here lies in noticing this *and* adjusting the separation valves accordingly, for human error plays a considerable role in the process. For example, during the experiment WMSs measurements have to be taken (this entails disconnecting the cables, moving them to the other place, connecting them again, and taking data), the water level in the tank must be maintained at its proper height, the weir pressure may not become too high, and chlorine has to be but in the tank in order to break apart the dye.

The report would become too elaborate if one would delineate the possible errors every single fluorescein data set may contain in this report, so we will not do that. I did, however, re-measure fluorodata that had to be redone 'for sure' (there were ones of greater priority of being redone than e.g. Fig. 4.7), which in practice meant remeasuring everything. In the end, five data sets of 64 remained which had distinctively unclear fluorescein dye concentration data. These were $Re_{DH} = 4 \cdot 10^4$ at $20\,slpm$, $Re_{DH} = 8 \cdot 10^4$ at $[0, 50, 100, 150]\,slpm$, all at the $20\,mm$ gap height.

Another way of looking at the mixing behavior is by looking at how mixing changes with Reynolds while keeping a gas flux constant. The two graphs in Fig. 4.8 show that the single-phase case remained at constant mixing rates. Both graphs show somewhat same behavior, although the $20\,mm$ case is 'flatter'. The low flux cases ($Q_g = [10, 20]\,slpm$)

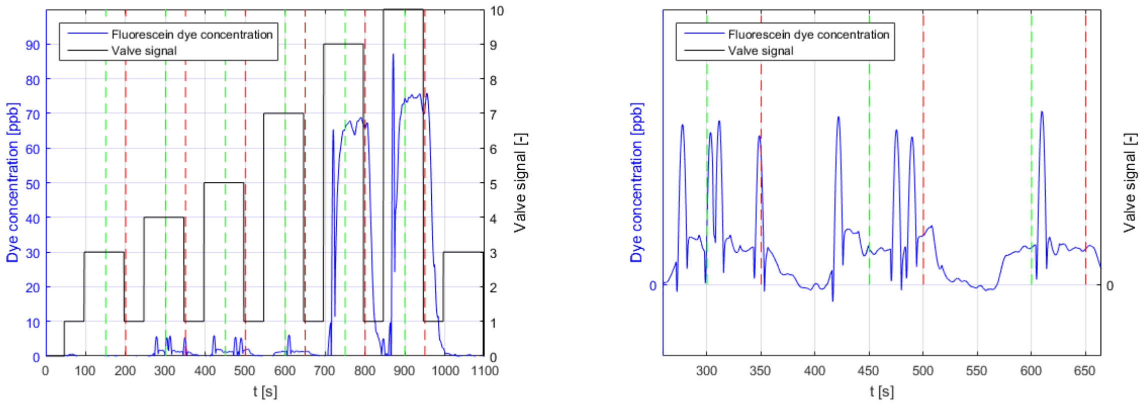

(a) Total.

(b) Zoomed in at the *ao* measurements.

Figure 4.7: Fluorescein data for the $20\,mm$ gap case at $Re_{DH} = [8 \cdot 10^4, 8 \cdot 10^4]$ and $Q_g = 150\,slpm$.

show an increase in mixing rate when increasing Re_{DH}. The opposite is true for the higher flowrates ($Q_g = [50, 100, 150]\,slpm$). It is difficult to draw quantitative conclusions from these graphs when it is known that there are data sets with inaccurate dye data and x-y mixing disparities. Qualitatively, however, we can speculate in which direction the gas flowrate has to be adjusted in order to optimize mixing at a certain Reynolds number, or how the Reynolds number must change when the gas flowrate is constant. This may be helpful in industrial design applications, if more accurately quantified in the future.

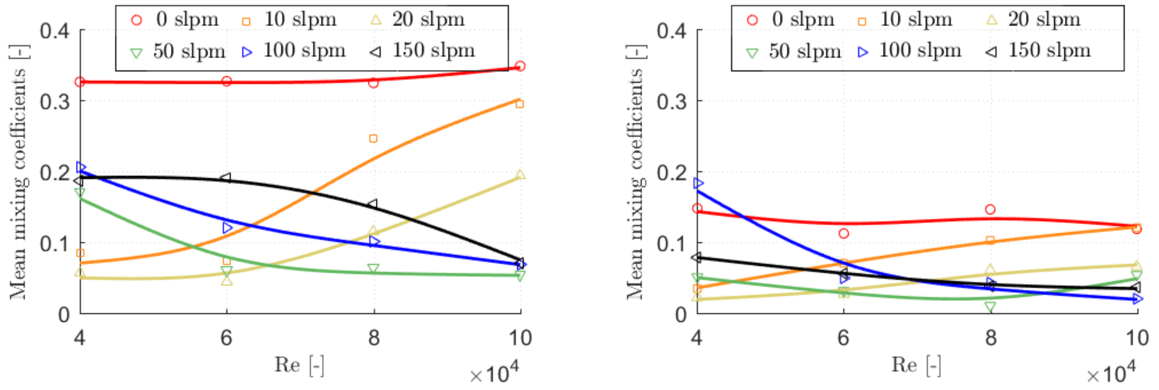

(a) $50\,mm$ gap height

(b) $20\,mm$ gap height

Figure 4.8: Reynolds number plotted against the mixing coefficients for different gas fluxes.

4.1.3 Physical perspective

The single-phase case studies showed that large vortex structures were the primary cause for integral mixing. Extending the study to two-phase flux by adding gas showed that bubbles broke up these structures, thus inhibiting mixing. As the volumetric flowrate of the gas in the water column increased, mixing in turn decreased. This happened, however, up to a point: a local minimum just below $\beta \approx 0.08$. Two main questions arise from these observations. *How does an increase in gas flowrate initially lead to a decrease in mixing?* (1). *How does an even further increase in gas flowrate at a certain point lead to an increase in mixing again?* (2).

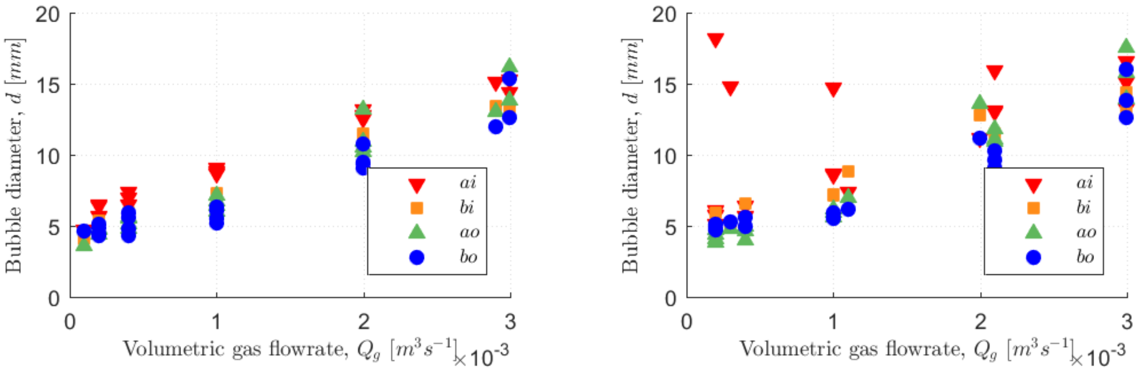

(a) $50\,mm$ gap height

(b) $20\,mm$ gap height

Figure 4.9: Bubble diameters d for the different channels at all Reynolds numbers plotted against the volumetric gas flowrate Q_g. *Note: Fig. 4.9(b) contains inaccurate ai WMS data due to errors during calibration.*

To get a better understanding of what happens physically, we could try to look at what happens with the bubble size as the gas flowrate increases. Take a look at Fig. 4.10 to see all bubble sizes plotted against the volumetric gas flowrate. The figures show a somewhat linear increase of the bubble size with increasing gas flowrate. No interesting observations can be made here which relate to the local minimum observed in the mixing figures.

However, when plotting the diameter against the volumetric quality β, we *do* notice something significant—two things, actually. First, the data seems to spread as the liquid velocity is also taken into account now, which is fairly straight-forward to understand. Second, a little above $\beta \approx 0.1$ we observe a sudden shift in bubble size, both for the $50\,mm$ gap height case, and the $20\,mm$ one. This sudden shift happens to be around the same area at which the local minimum in the mixing figures occurs. To see whether this jump is actually real, a higher resolution study around $\beta = 0.1$ has to be performed. If so, this jump might explain the increase in mixing again, as it could indicate a change in flow type entirely. We can distinguish between two different regions regarding mixing behavior—one where the volumetric quality is inversely proportional to mixing behavior (region I), and one where the volumetric quality is proportional to mixing behavior (region II)—which can be physically substantiated by the apparent shift in bubble size. Why

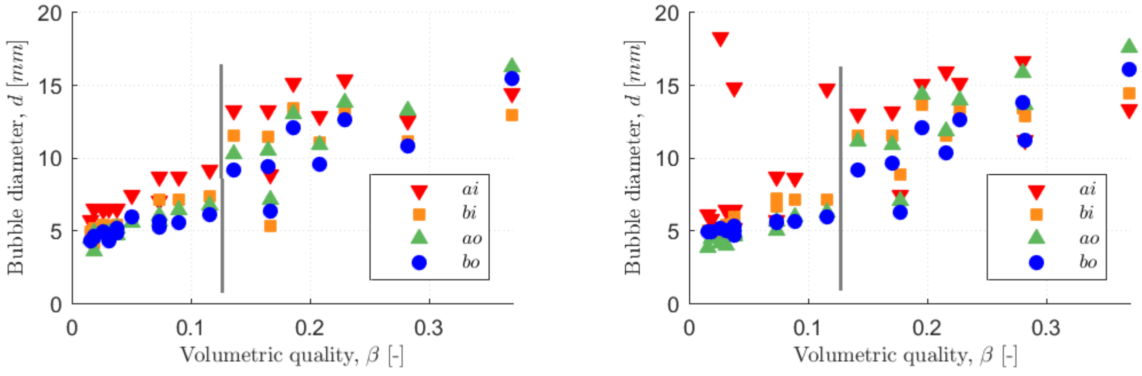

(a) 50 mm gap height (b) 20 mm gap height

Figure 4.10: Bubble diameters d for the different channels at all Reynolds numbers plotted against the volumetric quality β. *Note: Fig. 4.10(b) contains inaccurate ai WMS data due to errors during calibration.*

sudden significantly larger bubbles allow for more mixing remains unclear. It may be due to the large scale structures being broken up less, but for that we need to look at visual data first (which we do have, yet is outside the scope of this report) which may give us some hints in the right direction. One might look, for example, whether there is a change in flow regime corresponding with the change in bubble size (that is by looking at two-phase flow regimes that look like Hewitt & Robertson (1969)).

4.2 Mixing inequality

Another point of discussion was the fact that there was a difference in mixing from channel A to channel B, x, than the other way round, y. These points can be seen in Figs. 3.11 and 3.13 at low-Reynolds, most prominently seen at gas fluxes of $Q_g \approx [1, 2, 3]\, m^3 s^{-1}$. Before speculating on the root of the problem, let us first determine whether we have other physical evidence which shows unequal mixing. When more liquid would go from channel A than channel B, mass conservation would say that channel B would measure a larger flow water going out than A would. Is it possible to correlate mixing disparity with a disparity of the flow going out? Let us look at the differences in x and y and the differences in liquid flow out in channels A and B.

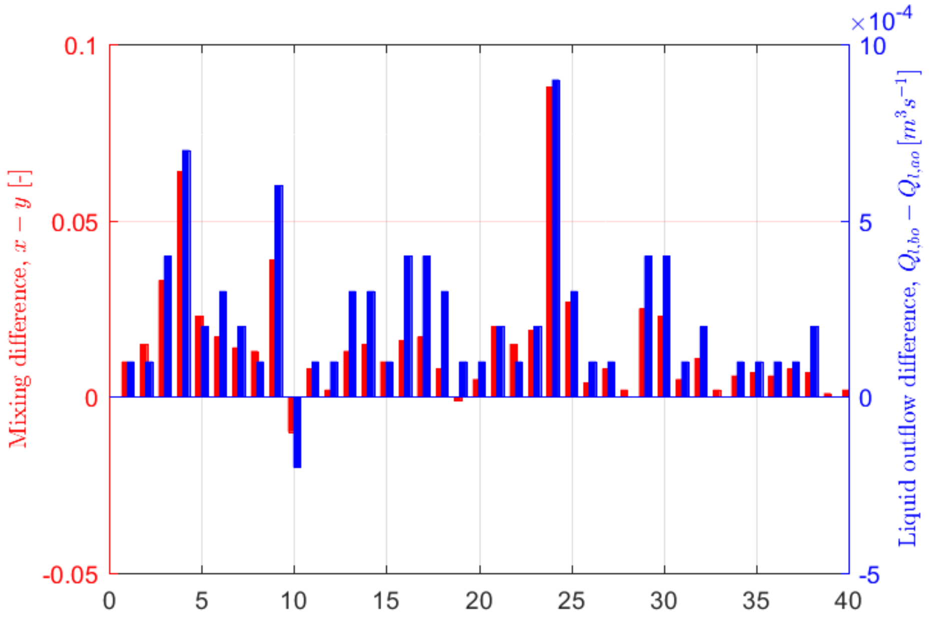

Figure 4.11: Bar plots of the mixing differences, $x - y$, laid out next to the differences in liquid outflow, $Q_{l,bo} - Q_{l,ao}$, for forty different data sets. The first twenty data sets denote the $50\,mm$ gap case; the remaining twenty the $20\,mm$ gap case.

Fig. 4.11 shows that mixing disparity indeed was physical, as the outlet pumps at channel B had to pump out more water per unit time. There also happened to be a case where $y > x$—this was at $Re_{DH} = [8 \cdot 10^4, 8 \cdot 10^4]$ and $Q_g = 10\,slpm$—which was followed by a negative liquid flow difference as well. Many cases showed the mixing difference to be proportional to the liquid flowrate differences. The reason why the differences do not coincide on the graph, is probably because of the fact that the liquid flow out was adjusted manually, depending on the rate at which the pressures in the weir boxes change.

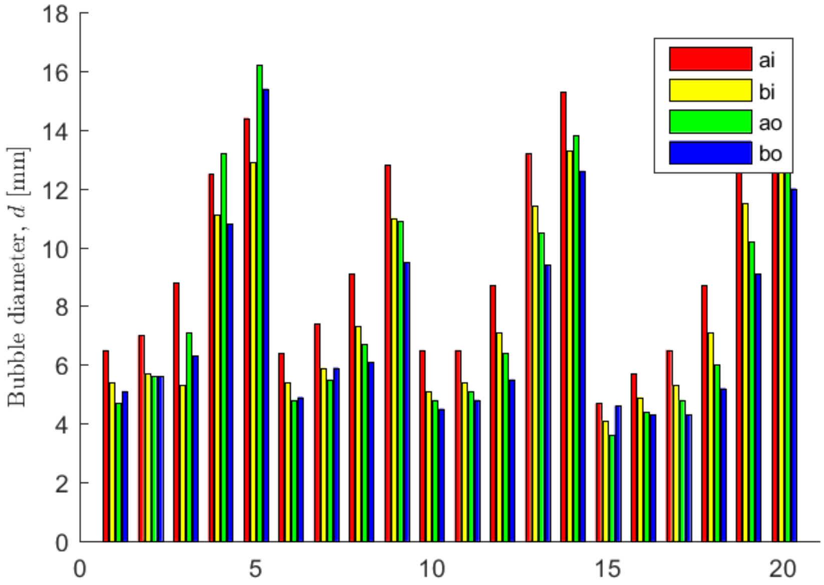

Figure 4.12: Bubble diameters per channel location. Gap height: 50 *mm* gap height.

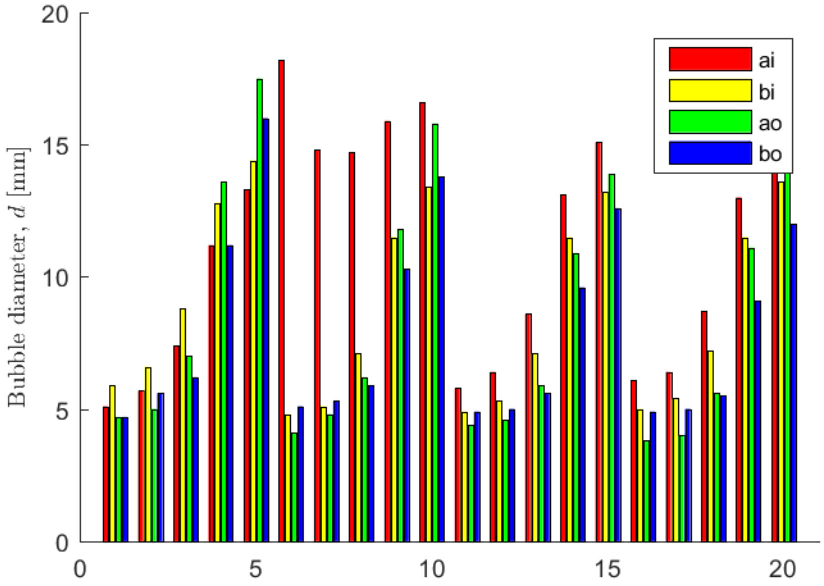

Figure 4.13: Bubble diameters per channel location. Gap height: 20 *mm* gap height. The data sets 6 to 10 contain erroneous WMS data for channel *ai*, as already pointed out earlier in the report.

As it has just been confirmed that mixing indeed is physical, it is due now to look for the cause of the problem and its solution. The channel A WMSs were different from the ones at channel B. We were using 100 μm diameter wires for the WMSs at channel *ai*, whereas the wires of all the other channels (i.e. *ao*, *bi* and *bo*) had wires of 200 μm in diameter.

This had initially been set up this way in order to examine whether different wire sizes would affect mixing at all or not. It may be that the mixing disparities were caused by this particular difference. Figs. 4.12 and 4.13 show the different bubble sizes per channel per data set. In a large majority of the cases, bubbles at channel ai were repeatedly shown to be larger than those at bi, which happens to be the case at the outer channels as well. Larger bubbles through channel A with the same total volume ($\int Q_g = N \cdot \bar{V}$, where N is the total amount of bubbles and $\bar{V}$ the average volume of a bubble) would mean a smaller number of bubbles through ai, so $N_{ai} < N_{bi}$. How a smaller number of larger bubbles could lead to more liquid escaping than coming in, remains unclear. Fewer, larger bubbles have a smaller total surface area, which would mean less liquid-gas interaction. Could it be that the larger bubbles have a larger displaced mass (meaning a larger buoyancy force), which means a larger vertical velocity component, and a smaller disruption of the large scale structures of the left side of the channel as horizontal movement is reduced? As the left-originating structures are less disrupted, left-to-right mixing would be stronger than right-to-left. Of course, it would require further research to test this hypothesis. Quite frankly, we do not know whether the difference in bubble size is a cause for the mixing disparity yet in the first place. Future research will give us an answer, as the WMS at ai will be replaced with one that has wires of similar diameter to the WMSs at ao, bi, and bo. Note: the two subsequent WMSs per channel will also be positioned closer together—they are spaced $50\,mm$ apart now—as to increase cross-correlation values, and thus obtain more reliable velocity data. Another future research step is to incorporate dual-tip optical probes within the set of sensors used, in order to be able to perform a more satisfactory velocity validation.

Chapter 5

Conclusions

Injection of nominally monodispersed air bubbles into adjacent, vertical flow channels connected by a narrow gap has been shown to drastically decrease the liquid mixing and mass transfer between the channels. The amount by which mixing is inhibited depends on the combination of injected gas flux, the Reynolds number, and the gap height. The main mechanism of reducing the mixing appears to be the inhibition of the formation of large coherent structures explicitly observed at the single-phase cases. Indications of preferred mixing conditions have been found using the measurements performed. Mixing was shown to collapse across a range of Reynolds numbers with respect to the volumetric quality, or the ratio of gas and liquid in the system, as well as with the two different gap heights studied. The inhibition number seemed to collapse with the volumetric quality as well, which was a way of collapsing the data without using a length scale. Visual observations of bubbles being convected between the channels along with the water due to their entrainment in the vortices were reviewed, and will be explored further to aid in the understanding of the reduced mixing for multi-phase flows as compared to the single-phase flows.

Additionally, the researchers are further exploring the parameter space, including varying gap heights and flow rates, to further develop the physical understanding of the multi-phase mixing phenomenon. We suggest higher-resolution measurements gap heights in particular, so that we may find more information on stacking mixing values with the gap height. Acquisition of additional data, analysis or the results accompanying CFD effort (by researchers other than the ones mentioned in this report), and more detailed comparison between the experimental and CFD data are ongoing.

Furthermore, in trying to solve the mixing disparities found in some data sets, future research will start using only one type of WMSs for all channel positions. On top of that, bringing the WMSs closer together will also help in obtaining higher cross-correlating values which are needed for velocity measurements. Integrating optical probe measurement into the system will help in obtaining more accurate velocity measurements as well. Finally, as a few data sets have been found to contain fluorescein dye data that contained inaccuracies, it is further suggested to perform some remeasurements of the corresponding data sets.

Part 2: Besides research

Chapter 6

Brief reflection

Disclaimer: informal English

The Marine Hydrodynamics Lab (MHL) is located at University of Michigan's Central Campus, an old building that the university will probably be renovating in the near future. The 'employer' who hired me was the Steven Ceccio, professor of Naval Architecture and Marine Engineering (NAME) and 'Vincent T. and Gloria M. Gorguze' Professor of Engineering. During four months of my stay, I had only seen him once for no more than ten minutes. He asked me whether I was learning anything new, to which I replied: "*Yes, I think so*," to which he responded: "*Good. As long as you learn new things, you're doing fine.*" At that point, however, I had been working with optical probes that I could not get to work for three weeks straight, so I wasn't sure about future 'learning' anymore. I don't think he realized I was wasting three weeks of my time. In any case, in reality my Prof. Ceccio was as much employer as I had progress working on the optical probes (OPs).

James Gose, a PhD-candidate at the department, supervised by Ceccio, was appointed as my supervisor, and was to my feeling my actual employer. He picked me up from home the first week I arrived, still during winter-break to show me around town, and, as time past by, guided me in the process of understanding the experimental set-up we were dealing with. This experimental set-up was as big as the entire laboratory space I worked in. It needs time for one to be able to process everything. Fortunately, there was another person at the lab, Elisabeth Callison, who was already acquainted with most of the space, so I had at least one person who could help me out when my supervisor was not around. And, quite frankly, I spent almost half of my days alone in the lab. James had a *very* busy schedule as he was working on his PhD research and had other projects going on on top of that, and Elisabeth was a Master's student who still had classes to attend and exams to study for. There were others working in the same building doing other kinds of research, but with them I had minimum interaction: hellos, goodbyes, and short inquiries such as: "Have you seen Jimmy?"

I have to admit it was hard making myself useful in the beginning when I had no clue on what I was going to do. Even three weeks in, I did not know I had to be taking hundreds of WMSs measurements, for example. I did inquire James on the future, and he told me I could do some research in something I interested in (e.g. he spoke about putting a wing in two-phase flows and investigating its wake), but we ended up not being able to do that due to some time-consuming matters regarding the equipment we were dealing with, and two major setbacks I myself caused, unfortunately. As for the former, the OPs did not work, changing the WMS cables took a long time to do every time, and the test section sometimes leaked after changing the gap height or callibrating the camera. As for the latter, I once flooded the lab by not closing the freshwater inlet valve, and once drained the tank by not closing the drain valve. These were my notes for the day I found out:

> I apparently left the freshwater inlet valve open, which overflowed the tank during the weekend. Ellie and I worked on getting the tank clean that day, I removed a cracked flange (I tightened them too much the Friday before, which made it crack), and we assembled some parts of the sub-off (?) (that missile-looking construction). New parts for the flange will come in tomorrow, so that'll have to be fixed then. Hopefully we'll be able to run the facility by Wednesday again.

That had been written on 27-03-2017. Four days later, 31-03-2017, see what I wrote next:

> Tank is being refilled, because I left the drain valve open. Had a short talk with Jimmy about accountability. Took out the trash. Started WMS processing. Called Tectivity. E-mailed Tectivity. Worked on optimal flush and measurement times with the new volume of water that's in the tank. We started running the WMS data processing (40 data sets).

Those two mistakes cost us about a week in total in time, and happened within days of each other, so it was more than normal that James and I 'had a talk'. Things went better after that. James has always been very patient with me, and I appreciate that. Flash-forward two weeks later, 14-04-2017, something else happened:

> So today I'm changing those reading methods I talked about yesterday, and reproducing the figures, whilst making sure the C7 data is analyzed as to verify the soundness of the results we're seeing. Also, upon arriving at the lab the tank was pretty much empty. Strange, as all valves had been closed upon my leave the day before. There were still some tests going on after I left, so that may have caused it, I assume. This means that I will not be able to take any measurements today.

This time it was James who drained the tank, I found out later. That was unfortunate, but also funny. Anyway, you can read the appendix for an overview of all my lab notes, if you are interested in more short stories of the day. They provide a more detailed description of my daily activities.

Setbacks like these are great lessons in meticulousness. If there is one advice I could give to people doing experimental research—or work in general— then it would be the following.

> Always make check-lists.

Appendices

Appendix A

Brief report on OP problem

This appendix covers the steps taken as denoted in the manual provided by RBI (the manufacturers) and the complications encountered while doing so.

A.1 Initialization

We start the process of using the dual-tip optical probes with the following initial conditions:

- The optical probe is connected to a frame that holds the probe in place, which will be air initially. The frame can be adjusted in such a way that it can hold the tip of the probe in either air or water;
- Not a single probe cable is connected to the opto-electronic unit (OEU);
- The opto-electronic unit is not connected to the oscilloscope;
- The oscilloscope is turned on;
  - The voltage outputs are approximately -100 mV when just the cables are plugged in. The cables are not yet connected to the OEU.
- The OEU is turned on;
  - The lights of all six amplifiers are green;
  - All gain switches are switched to their lowest positions (i.e. G3);

Next, we go through the step plan given in the 'User's guide: Two-Phase Flow Equipment' which can be found at page fifteen of the manual, chapter 'Adjustment of the Opto-Electronic Unit Amplifier'. The following part will denote every step taken in setting up the optical probes, as well as all observations made during this process.

A.2 Set-up

1. **Initialization of the gain and of the zero**
   The gain switches are on their lowest positions. The coarse button is turned anticlockwise. Note that the buttons can be turned physically 'forever' as there is no physical 'stop'. Because of the fact that the OEU is not connected to the oscilloscope yet, we cannot see when the extremity has been reached. We do not connect the OEU to the oscilloscope yet, because this step is operation is denoted in step three of the process.

2. **Adjustment of the optimum emission current**
   Now, the two probe cables are connected to the OEU and the 'probe adjust' is used in order to just get the light the amplifier emits to be green, as step two in the manual suggests. There are no further observations.

3. **Adjustment of the signal zero**
   The OEU is connected to the oscilloscope. The voltage output of amplifier 1 (A1) shows a negative value.of around -3.5 V. Amplifier 2 (A2) outputs a constant voltage of a little less than 9 V; every amplifier that does not seem to work, shows this phenomenon. Next, the probe is put into the liquid. A1 now outputs a slightly different voltage, but A2 does not. The coarse and fine switches are used. A1 has been put to almost 0 V (30 mV). A2 does not do anything to the voltage output when turning the coarse or fine button. It says at the same value.

4. **Adjustment of the gain amplifier and 5. Fine adjustment of the signal**
   The probe is put back in air and no water remains on the probe tip. We use the gain switches to get an output of at least 5 V now. The gain switches are set to G2, as recommended by RBI in the manual, but with this we could not get the output to 5 V. Therefore, we first put at G1, turned the gain, and got it up to 3 V. This output, however has large standard deviations (e.g. it went from 3V to 1 V), so we put it back to G2. The problem here, now, is that we cannot get the output value up. Turning the gain is of no effect. To troubleshoot that, we adjusted the 'probe adjust' even more carefully, which solved this problem for A1. We incorporated step five for A1, and A1 works now. For A2, however, nothing worked.

   The following things have been tried to get A2 to change its output value, and were of no avail.

   - Put the green light closer at borderline;
   - Turned the gain button anti-clockwise;
   - Turned the gain button clockwise;
   - Switched the gain to G2 or G1;
   - Turned the OEU on and off for 30 seconds, 30 minutes, two hours and a day;

- Swapped the optical probe cables → the problem does not lie in the optical probes;
- Swapped the amplifiers (A1 and A2) → the problem does not lie in the cabling between A2 and the OEU plug;
- Swapped the oscilloscope cables → the problem does not lie in the oscilloscope
- Checked whether A2 outputs any voltage at all (it does) → the problem does not lie in the cabling

The electrician checked that the potentiometers were working and they did.

5. **Adjustments of the detection threshold levels**
   This part worked for both amplifiers. We got the low level threshold to 1 V and the high level to 4 V. No problems found there.

Note: the problems occurred with A2 occurred with two other amplifier units as well: three of the six units do not work.

Appendix B

Summary data tables

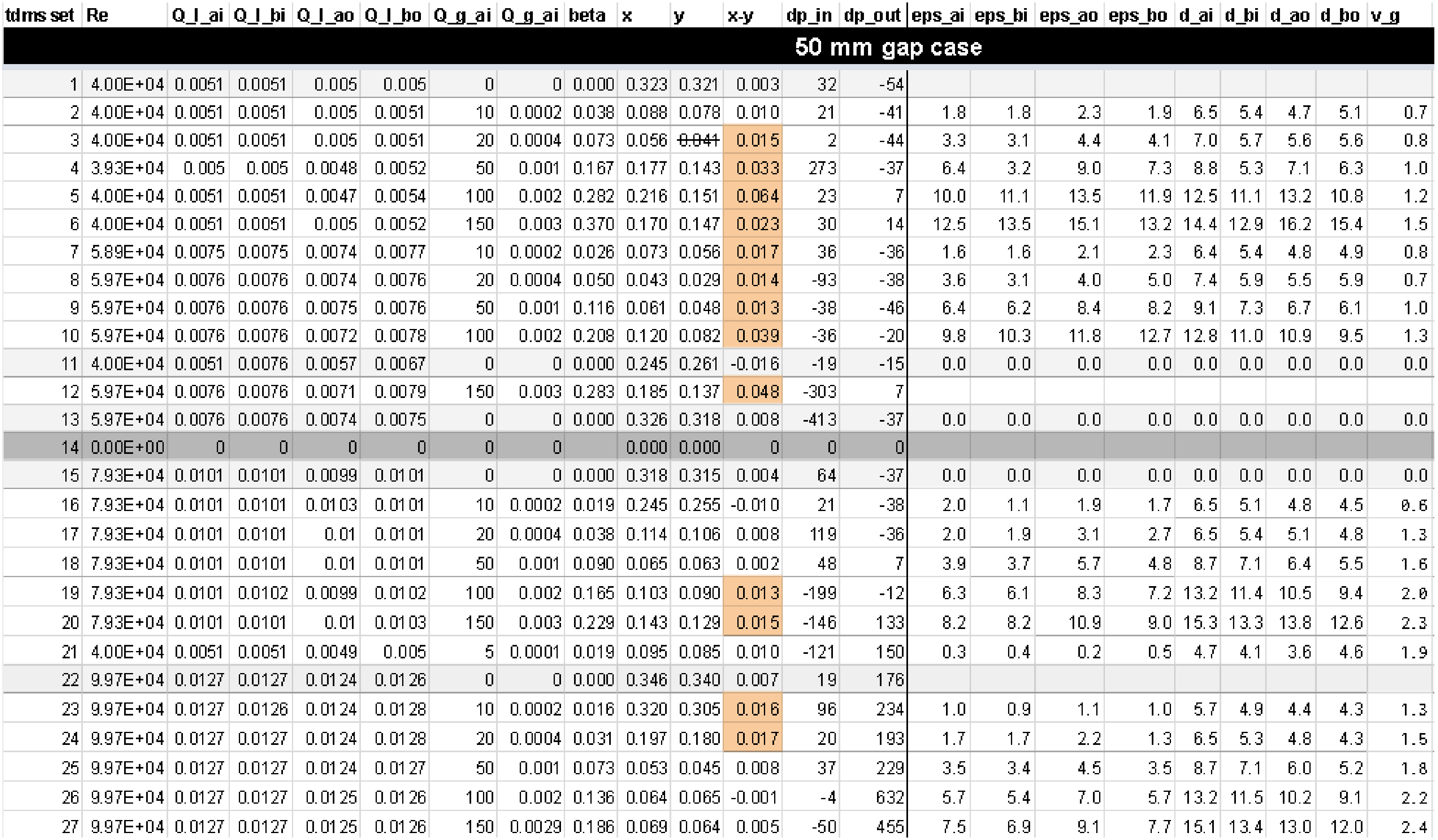

tdms set	Re	Q_l_ai	Q_l_bi	Q_l_ao	Q_l_bo	Q_g_ai	Q_g_ai	beta	x	y	x-y	dp_in	dp_out	eps_ai	eps_bi	eps_ao	eps_bo	d_ai	d_bi	d_ao	d_bo	v_g
50 mm gap case																						
1	4.00E+04	0.0051	0.0051	0.005	0.005	0	0	0.000	0.323	0.321	0.003	32	-54									
2	4.00E+04	0.0051	0.0051	0.005	0.0051	10	0.0002	0.038	0.088	0.078	0.010	21	-41	1.8	1.8	2.3	1.9	6.5	5.4	4.7	5.1	0.7
3	4.00E+04	0.0051	0.0051	0.005	0.0051	20	0.0004	0.073	0.056	~~0.041~~	0.015	2	-44	3.3	3.1	4.4	4.1	7.0	5.7	5.6	5.6	0.8
4	3.93E+04	0.005	0.005	0.0048	0.0052	50	0.001	0.167	0.177	0.143	0.033	273	-37	6.4	3.2	9.0	7.3	8.8	5.3	7.1	6.3	1.0
5	4.00E+04	0.0051	0.0051	0.0047	0.0054	100	0.002	0.282	0.216	0.151	0.064	23	7	10.0	11.1	13.5	11.9	12.5	11.1	13.2	10.8	1.2
6	4.00E+04	0.0051	0.0051	0.005	0.0052	150	0.003	0.370	0.170	0.147	0.023	30	14	12.5	13.5	15.1	13.2	14.4	12.9	16.2	15.4	1.5
7	5.89E+04	0.0075	0.0075	0.0074	0.0077	10	0.0002	0.026	0.073	0.056	0.017	36	-36	1.6	1.6	2.1	2.3	6.4	5.4	4.8	4.9	0.8
8	5.97E+04	0.0076	0.0076	0.0074	0.0076	20	0.0004	0.050	0.043	0.029	0.014	-93	-38	3.6	3.1	4.0	5.0	7.4	5.9	5.5	5.9	0.7
9	5.97E+04	0.0076	0.0076	0.0075	0.0076	50	0.001	0.116	0.061	0.048	0.013	-38	-46	6.4	6.2	8.4	8.2	9.1	7.3	6.7	6.1	1.0
10	5.97E+04	0.0076	0.0076	0.0072	0.0078	100	0.002	0.208	0.120	0.082	0.039	-36	-20	9.8	10.3	11.8	12.7	12.8	11.0	10.9	9.5	1.3
11	4.00E+04	0.0051	0.0076	0.0057	0.0067	0	0	0.000	0.245	0.261	-0.016	-19	-15	0.0	0.0	0.0	0.0	0.0	0.0	0.0	0.0	0.0
12	5.97E+04	0.0076	0.0076	0.0071	0.0079	150	0.003	0.283	0.185	0.137	0.048	-303	7									
13	5.97E+04	0.0076	0.0076	0.0074	0.0075	0	0	0.000	0.326	0.318	0.008	-413	-37	0.0	0.0	0.0	0.0	0.0	0.0	0.0	0.0	0.0
14	0.00E+00	0	0	0	0	0	0		0.000	0.000	0	0	0									
15	7.93E+04	0.0101	0.0101	0.0099	0.0101	0	0	0.000	0.318	0.315	0.004	64	-37	0.0	0.0	0.0	0.0	0.0	0.0	0.0	0.0	0.0
16	7.93E+04	0.0101	0.0101	0.0103	0.0101	10	0.0002	0.019	0.245	0.255	-0.010	21	-38	2.0	1.1	1.9	1.7	6.5	5.1	4.8	4.5	0.6
17	7.93E+04	0.0101	0.0101	0.01	0.0101	20	0.0004	0.038	0.114	0.106	0.008	119	-36	2.0	1.9	3.1	2.7	6.5	5.4	5.1	4.8	1.3
18	7.93E+04	0.0101	0.0101	0.01	0.0101	50	0.001	0.090	0.065	0.063	0.002	48	7	3.9	3.7	5.7	4.8	8.7	7.1	6.4	5.5	1.6
19	7.93E+04	0.0101	0.0102	0.0099	0.0102	100	0.002	0.165	0.103	0.090	0.013	-199	-12	6.3	6.1	8.3	7.2	13.2	11.4	10.5	9.4	2.0
20	7.93E+04	0.0101	0.0101	0.01	0.0103	150	0.003	0.229	0.143	0.129	0.015	-146	133	8.2	8.2	10.9	9.0	15.3	13.3	13.8	12.6	2.3
21	4.00E+04	0.0051	0.0051	0.0049	0.005	5	0.0001	0.019	0.095	0.085	0.010	-121	150	0.3	0.4	0.2	0.5	4.7	4.1	3.6	4.6	1.9
22	9.97E+04	0.0127	0.0127	0.0124	0.0126	0	0	0.000	0.346	0.340	0.007	19	176									
23	9.97E+04	0.0127	0.0126	0.0124	0.0128	10	0.0002	0.016	0.320	0.305	0.016	96	234	1.0	0.9	1.1	1.0	5.7	4.9	4.4	4.3	1.3
24	9.97E+04	0.0127	0.0127	0.0124	0.0128	20	0.0004	0.031	0.197	0.180	0.017	20	193	1.7	1.7	2.2	1.3	6.5	5.3	4.8	4.3	1.5
25	9.97E+04	0.0127	0.0127	0.0124	0.0127	50	0.001	0.073	0.053	0.045	0.008	37	229	3.5	3.4	4.5	3.5	8.7	7.1	6.0	5.2	1.8
26	9.97E+04	0.0127	0.0127	0.0125	0.0126	100	0.002	0.136	0.064	0.065	-0.001	-4	632	5.7	5.4	7.0	5.7	13.2	11.5	10.2	9.1	2.2
27	9.97E+04	0.0127	0.0127	0.0125	0.0126	150	0.0029	0.186	0.069	0.064	0.005	-50	455	7.5	6.9	9.1	7.7	15.1	13.4	13.0	12.0	2.4

Figure B.1: 50 mm gap

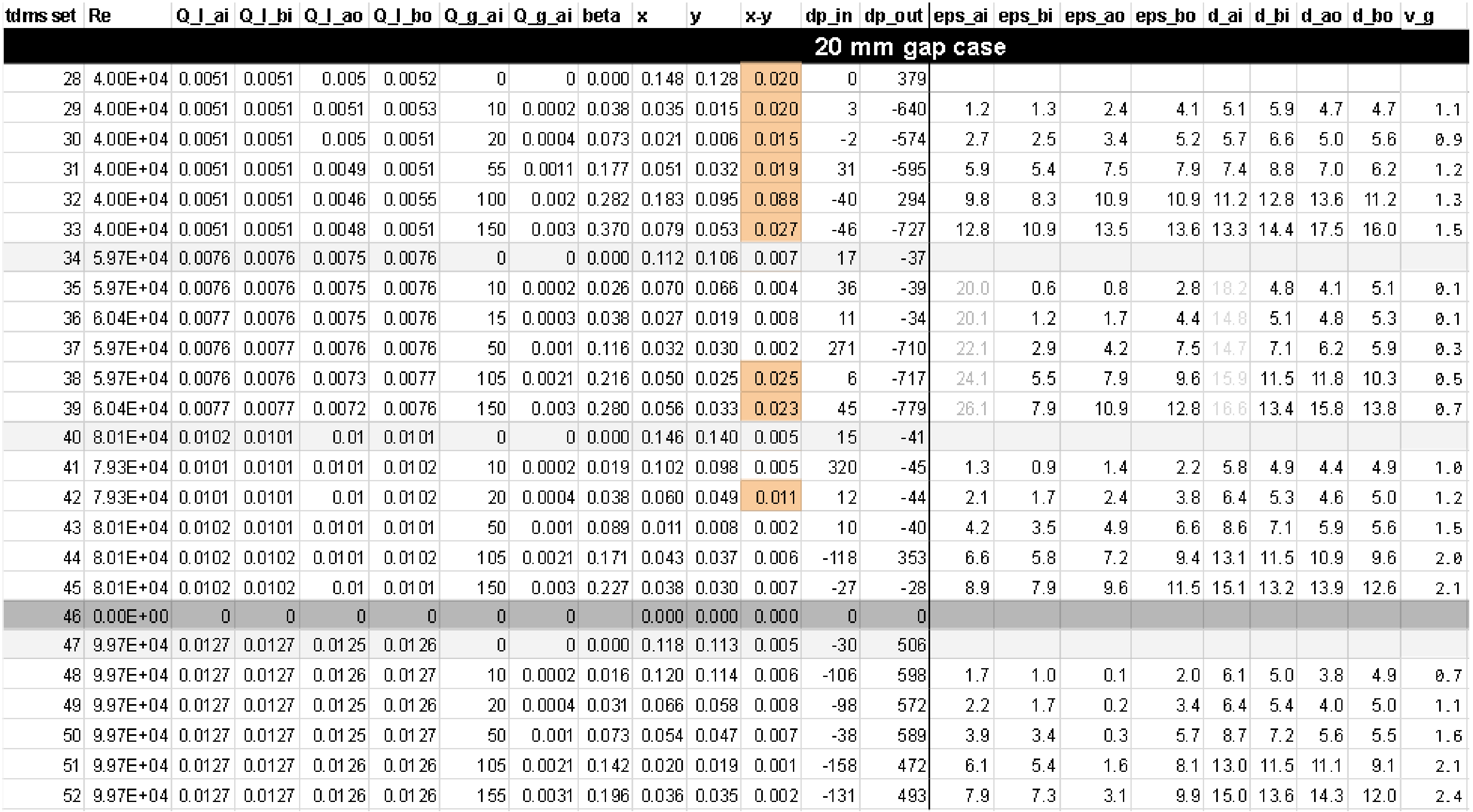

tdms set	Re	Q_l_ai	Q_l_bi	Q_l_ao	Q_l_bo	Q_g_ai	Q_g_ai	beta	x	y	x-y	dp_in	dp_out	eps_ai	eps_bi	eps_ao	eps_bo	d_ai	d_bi	d_ao	d_bo	v_g
20 mm gap case																						
28	4.00E+04	0.0051	0.0051	0.005	0.0052	0	0	0.000	0.148	0.128	0.020	0	379									
29	4.00E+04	0.0051	0.0051	0.0051	0.0053	10	0.0002	0.038	0.035	0.015	0.020	3	-640	1.2	1.3	2.4	4.1	5.1	5.9	4.7	4.7	1.1
30	4.00E+04	0.0051	0.0051	0.005	0.0051	20	0.0004	0.073	0.021	0.006	0.015	-2	-574	2.7	2.5	3.4	5.2	5.7	6.6	5.0	5.6	0.9
31	4.00E+04	0.0051	0.0051	0.0049	0.0051	55	0.0011	0.177	0.051	0.032	0.019	31	-595	5.9	5.4	7.5	7.9	7.4	8.8	7.0	6.2	1.2
32	4.00E+04	0.0051	0.0051	0.0046	0.0055	100	0.002	0.282	0.183	0.095	0.088	-40	294	9.8	8.3	10.9	10.9	11.2	12.8	13.6	11.2	1.3
33	4.00E+04	0.0051	0.0051	0.0048	0.0051	150	0.003	0.370	0.079	0.053	0.027	-46	-727	12.8	10.9	13.5	13.6	13.3	14.4	17.5	16.0	1.5
34	5.97E+04	0.0076	0.0076	0.0075	0.0076	0	0	0.000	0.112	0.106	0.007	17	-37									
35	5.97E+04	0.0076	0.0076	0.0075	0.0076	10	0.0002	0.026	0.070	0.066	0.004	36	-39	20.0	0.6	0.8	2.8	18.2	4.8	4.1	5.1	0.1
36	6.04E+04	0.0077	0.0076	0.0075	0.0076	15	0.0003	0.038	0.027	0.019	0.008	11	-34	20.1	1.2	1.7	4.4	14.8	5.1	4.8	5.3	0.1
37	5.97E+04	0.0076	0.0077	0.0076	0.0076	50	0.001	0.116	0.032	0.030	0.002	271	-710	22.1	2.9	4.2	7.5	14.7	7.1	6.2	5.9	0.3
38	5.97E+04	0.0076	0.0076	0.0073	0.0077	105	0.0021	0.216	0.050	0.025	0.025	6	-717	24.1	5.5	7.9	9.6	15.9	11.5	11.8	10.3	0.5
39	6.04E+04	0.0077	0.0077	0.0072	0.0076	150	0.003	0.280	0.056	0.033	0.023	45	-779	26.1	7.9	10.9	12.8	16.6	13.4	15.8	13.8	0.7
40	8.01E+04	0.0102	0.0101	0.01	0.0101	0	0	0.000	0.146	0.140	0.005	15	-41									
41	7.93E+04	0.0101	0.0101	0.0101	0.0102	10	0.0002	0.019	0.102	0.098	0.005	320	-45	1.3	0.9	1.4	2.2	5.8	4.9	4.4	4.9	1.0
42	7.93E+04	0.0101	0.0101	0.01	0.0102	20	0.0004	0.038	0.060	0.049	0.011	12	-44	2.1	1.7	2.4	3.8	6.4	5.3	4.6	5.0	1.2
43	8.01E+04	0.0102	0.0101	0.0101	0.0101	50	0.001	0.089	0.011	0.008	0.002	10	-40	4.2	3.5	4.9	6.6	8.6	7.1	5.9	5.6	1.5
44	8.01E+04	0.0102	0.0102	0.0101	0.0102	105	0.0021	0.171	0.043	0.037	0.006	-118	353	6.6	5.8	7.2	9.4	13.1	11.5	10.9	9.6	2.0
45	8.01E+04	0.0102	0.0102	0.01	0.0101	150	0.003	0.227	0.038	0.030	0.007	-27	-28	8.9	7.9	9.6	11.5	15.1	13.2	13.9	12.6	2.1
46	0.00E+00	0	0	0	0	0	0		0.000	0.000	0.000	0	0									
47	9.97E+04	0.0127	0.0127	0.0125	0.0126	0	0	0.000	0.118	0.113	0.005	-30	506									
48	9.97E+04	0.0127	0.0127	0.0126	0.0127	10	0.0002	0.016	0.120	0.114	0.006	-106	598	1.7	1.0	0.1	2.0	6.1	5.0	3.8	4.9	0.7
49	9.97E+04	0.0127	0.0127	0.0125	0.0126	20	0.0004	0.031	0.066	0.058	0.008	-98	572	2.2	1.7	0.2	3.4	6.4	5.4	4.0	5.0	1.1
50	9.97E+04	0.0127	0.0127	0.0125	0.0127	50	0.001	0.073	0.054	0.047	0.007	-38	589	3.9	3.4	0.3	5.7	8.7	7.2	5.6	5.5	1.6
51	9.97E+04	0.0127	0.0127	0.0126	0.0126	105	0.0021	0.142	0.020	0.019	0.001	-158	472	6.1	5.4	1.6	8.1	13.0	11.5	11.1	9.1	2.1
52	9.97E+04	0.0127	0.0127	0.0126	0.0126	155	0.0031	0.196	0.036	0.035	0.002	-131	493	7.9	7.3	3.1	9.9	15.0	13.6	14.3	12.0	2.4

Figure B.2: $20\,mm$ gap

Appendix C

Documentation of activities

Disclaimer: informal English, personal notes and thoughts as they were written down at the moment. No original note has been altered after it had been written down.

09-01-2017

> Started setting up MATLAB script for data processing, moved furniture to and fro, set up a table, and worked on calibrating the optical probes, yet without success.

10-01-2017

> Finished the two lab trainings. Had to redo one because of some technical issue. Had the J1-visitors check-in.

11-01-2017

> Continued work on MATLAB script. Added liquid and temperature data, and set up more formulas.

12-01-2017

> Read about WMS, optical probes and spent majority of the time testing out probes. Of the first probe tested no. 2 did not seem to work. Note: using the gain switches on order to adjust voltage levels helped in order for the voltage to increase. This made no. 1 work; no. 2 did not despite multiple efforts. No. 1 of the second probe works. No. 2 of the second probe did not work (I couldn't get it to 5V) for a long time, until I decided to adjust the 'adjust probe' setting. The third probe did not seem to work at all: I could not calibrate the sensor in that it would signal 5V when exposed to air. It seems that getting it to 0V in water is done relatively easily compared to making the output 5V when in air.

13-01-2017

I managed to calibrate the third probe properly now as well. The problem really lies in how one works the ‘adjust probe’ setting. You must handle it with enormous delicacy. I can get the high level threshold to be 4V using the multimeter, but haven’t found a way to adjust the low level to 1V. Turning the ‘low level’ button is of no avail. Might it be an idea to position the probes both facing downwards and upwards as in to also measure downward moving bubbles? Many bubbles move down in transitioning or churn-turbulent flow. In our experiment, however, we’ll be dealing with bubbly flow only.

16-01-2017

I had as a goal to set up all the three probes to the amplifier, properly calibrate them, and read data out from the computer using the associated software. Problems ensued when the second and third plug did not give any response when used. The problem did not lie with the optical probe, nor the oscilloscope. It is most likely the amplifier that needs some troubleshooting. The fourth socket was working, until it suddenly did not work anymore. ‘Suddenly’ as in: I changed the connection from the fourth socket to the second and to the third (to no avail), after which I placed it backed to the fourth socket–the settings of the fourth station had not been tampered with, mind you. Then, however, the fourth also failed. The voltage stayed at 10V, and was not influenced by turning the gain, coarse or fine button, nor when changing medium (air-water). When all that failed (which was after the greater part of the day), I decided to collect some literature on optical probes, in order to improve my understanding on the subject.

17-01-2017

In most papers I am reading that single point (or ‘monofiber’) optical probes are very inaccurate and rarely used. It does not tell you the direction in which the bubble propagates, nor the velocity. One paper says that using a two-point probe is not reliable as well, and even proves it (Xue et al.). By the way, assuming a spherical bubble seems to be a bad idea, as most bubbles in a bubble column are more ellipsoidal. A two-point probe inaccurately indicates chord length and bubble velocity, as the orientation of the bubble greatly affects the measured results. Only when the bubble attacks the probe head-on (i.e. with its velocity vector exactly in the direction of the probe), this won’t be a problem. Therefore, we need to make sure all bubbles indeed do traverse in one and the correct direction. Tried compiling a step-by-step manual for using the optical probes. I added some steps and comments, and tried to find solutions for the fact that sockets two, three and four do not work. Socket four worked yesterday. The reason why it does not work anymore, is very much unclear. All sockets do not respond to switching the 'adjust probe' setting at all, whilst the other ones do heavily do so.

18-01-2017

Continued trying to fix the other probe; now with Jimmy, but again, nothing working. We allocated to problem to the electrician of the lab. I have read some papers, connected the wire mesh cables and started working on a SolidWorks part in order to be able to connect all the wire mesh cables at once. It's like a splitter. I didn't have access to the Caen network, so I had to download and install the software on my laptop, which took approximately 2.5 hours.

19-01-2017

Finished the SolidWorks part. Jimmy wasn't here to check, so perhaps there will be some adjustments tomorrow. There were no further tasks given; my supervisor told me that I could then just take it easy today. He could not be around in the lab.

20-01-2017

Helped cleaning out the back - sorting cables, throwing away old and unused items, and so on. Tested the probes again, and they did not work. Wrote a small report on that, which has been sent to probe's manufacturers. Also, Jimmy gave me a tutorial on how the WMS software works.

23-01-2017

Tried to set up the optical probes. Whenever you get one value right (either 0 V in water or 5 V in air), putting the probe in the opposite medium only very slightly influences the voltage output. You would think that might have to do with the gain being too low, so I lowered the gain significantly, after which I made the output 0 V again when in water. After that, I tried to put it to 5 V in air, which I succeeded in, but when putting it back to water again, it only lowered with 0.5 V or so. 1 V max. Tried changing the threshold levels, but that would mean I'd do something different from what the manual said I should do. I also tried using the mono-fiber optical probe. Now amplifiers one and five do not work anymore as well, so I used number six to try it out. I got the exact same problem. The jump between water and air is just too low in order to accurately register the existence of a bubble in water.

24-01-2017

Worked with the optical probes the entire day. Nothing worked. Reinstalled the dual-tip optical probe, which also did not work, obviously. Still no response from RBI (the company that manufactures the optical probes and the system around it (opto-electronic unit).

25-01-2017

WMSs couldn't be pulled out, so I replaced the O-ring, reattached the frames and cleaned the WMS wires through the open window. After that I reinstalled the window, rewired the WMS cables, and did a test run with Ellie. We started doing some data processing: she using the data from the camera, and I from the WMS. RBI responded towards the end of the day. Nothing beneficial from their side. We suggested to call or Skype.

26-01-2017

RBI responded by saying the problem lies in the electronics, which was what we had figured out as well. They want the unit to be sent to them, so that they may fix it. Further, I've incorporated (test-) WMS data files in the main MATLAB processing file. Both WMS and TDMS data are now used to find different system parameters.

27-01-2017

The opto-electronic unit has been sent away. Worked on matlab files that generate velocity files from void files. Made it so that that goes automatically. Also, I made functions that read and unpack TDMS data files. I at least still need to:

- Make the function execute other executables than velocity.exe only
- Make the main processing matlab file in such a way that it can cope with the different blocks
- Make a function file that makes one big time-averaged block
- Look at auto-correlation

30-01-2017

We ran the entire test facility. Data has been collected. Three data sets of one and the same experiment will be analyzed. We wanted to do another experiment at different gas fluxes, but then the WMS sensor did not work anymore. After that I started processing the WMS data in the WMS FrameWork software.

31-01-2017

Continued processing the WMS data in MATLAB.

01-02-2017

Automated WMS processing in MATLAB. I still need to at least work on:
- Adding cross-correlation;
- Not having to put in all the filenames myself;
- Create a naming convention for the .tdms and wms files
- Correct formulas

02-02-2017

- Automation and data collection

03-02-2017

- Automation

06-02-2017

- Data collection and troubleshooting sensor 2 measurements errors

→ Sensor 2 suddenly measured bubbles to be far greater than they actually were, showing peaks at diameters as large as 120 mm. We ran the experiment three times, and each time the distribution was significantly off.

07-02-2017

Still dealing with the same problem. Moved sensors to bi, where everything worked fine. Moved sensors to ai again, where everything worked fine again. I suspect it simply had to do with corrupt .mes files?

08-02-2017

Performed several measurements, where we again found peaks at 200 mm diameter. After that bubident.exe crashed time and time again, which may have had to do with corrupt files. The cause of the problem remains unknown. After gathering new .mes files, bubident.exe did not seem to crash anymore, nor did the .mes files show any corruption when examining the bubble size distributions. When that worked, we moved the sensors to ao, performed some measurements there, and processed the data. Ellie eventually put a report together wherein some of these data are given.

09-02-2017

Data collection of 121 gpm flow. Afterwards I tried data processing, which did not work. Data files were corrupt.

13-02-2017

Data collection of 80 gpm flow. Data got processed, and compared with camera data. We only looked at low gas fluxes (¡1 slpm). At 1 slpm gas flux in and 3 slpm gas flux in, data appeared to be very inaccurate. WMSF determined that there were bubbles of 110 mm in diameter, which cannot be true. The area eq. diameter is calculated to be approximately 5 mm (correct range) and 20 mm (incorrect range), while the volume eq. diameter is calculated to be approximately 6 mm (correct range) and ¿100 mm (incorrect range).

14-02-2017

Trying to understand cross-correlation values. Sought maxima and linked them to velocities. I've seen some high velocities linked to cross-correlation low maxima (0.01), which I find rather strange, as I expected values to approach unity.

15-02-2017

Did thirty measurements at location ai at ten different gas and three liquid fluxes. After that, all data has been processed into .a, .b, .velxy, ...-files. Mind you, we're talking about over 24 GB of datapoints that had to be processed in MATLAB. The only thing that crashed was datarun˙wms˙006˙Sensor2. I do not have files of that one. For some reason, that .mes file is corrupt. Bubble identification crashed every single time. This data run was the one where the liquid flow rate was 121 gpm, and the gas flow rate 10 slpm.

16-02-2017

Processed data.

17-02-2017

Processed data.

20-02-2017

We took measurements over the weekend. 44 data sets. Processed them. WMS mount was created.

21-02-2017

Incorporated drift fluxes in the data processing file.

22-02-2017

Added 8-point velocity averaging and drift fluxes corrections. Looked at mass balance. Adjusted MATLAB functions to facilitate difference velocity adjustment methods and different velocity threshold levels. Compared drift fluxes to Ishii (1977). Connect WMS cables to WMS mounts.

23-02-2017

Additional data collection and processing.

24-02-2017

ibid.

06-03-2017

Started collecting data with the gap open plus processing it. It needed adjustments in the code now.

07-03-2017

Coding.

08-03-2017

Again data collection today. Did the open gap case at 81 gpm and two different gas fluxes.

09-03-2017

Collected data for two different gas fluxes again at 81 gpm. Data processing took until 10.30 PM.

10-03-2017

Had to collect data at 81 gpm again, for the highest has flux (150 slpm), because the WMS gave some errors yesterday. They still give them today, but we'll continue and hope the data is not too corrupt. "Some Framen may be corrupted."

11-03-2017

Collected data for wide gap mixing case for liquid fluxes of 121 gpm. We initially thought that because of the fact that it'd take 20 minutes to take .tdms data, we could just switch the WMS cables from ao, bo, bi to ai in the meantime. But it took longer than we initially thought. A personal remark was that it is rather physically demanding to switch WMS ports every single time. That day I did it sixteen times. That day before sixteen times as well (four ports times four different gas fluxes). The other four gas fluxes were done the days before (April 8th and 9th).

12-03-2017

Processed Saturday's data. WMS measurement files were not all that good. During measurements eleven out of fifteen .mes files were damaged (reason why was unknown), and when processing these files, 7/15 had crashes during bubident.exe, which means we do not know the bubble sizes of these seven files (these were only Sensor 2 files; we do have all the Sensor 1 bubble data).

13-03-2017

From now on we needed everything to be post-processed. We needed mixing data. I used relations that were formulated by Simo earlier for determining the amount of mixing from channel A to channel B and vice versa. Before doing so, I analytically checked these equations by solving them myself first. I put the mixing relations into MATLAB. We also took some unbalanced mixing data.

14-03-2017

When sampling the concentration of the fluorescent dye, you see that it takes some time for the measurement to become reach a quasi-steady state. The sensor overshoots when changing valves, which had to be taken into account as well when determining the concentrations. We simply decided not to take these measurements into our calculations, which in my opinion is very OK.

15-03-2017

What we now want to discover are the physical variables that influence the mixing process. So for that I looked at different gas fluxes, pressures, bubble sizes, void fractions, drift fluxes, pressure differences between channels, bubble diameter differences per channel, and bubble velocities.

16-03-2017

Further looked at what could influence mixing. It seems to be the case that mixing from A to B was stronger than B to A, and we wanted to see what caused that. We could not find it in pressure differences in the inlet channels, nor bubble sizes. I have not yet looked at differences in void fractions. Perhaps I should do that too.

17-03-2017

Tried to further understand what really influenced bubble mixing. I found that with higher gas flux, you'd have higher void fractions and larger bubbles (meaning that bubbles coalesce into larger ones). The no-gas case had the highest mixing; adding bubbles significantly inhibited the mixing process, although increasing gas flux does nuance this inhibition. We suspect the bubble distributions the needle affects mixing as well. I also added a concentration decay factor to account for dye breaking up between inlet and outlet.

20-03-2017

Took three cases of .tdms data and twenty wms data sets.

21-03-2017

Took first case of .tdms data. Waited for a while to get the dye concentration lower. Worked on processing yesterday's WMS data in the meantime. When checking for concentrations, they did not seem to have diminished sufficiently. Checked vacuum pump pressure, made sure fresh water was coming in the tank, and made sure that only water entered the fluorometer. Still no decrease in concentration a couple of hours later. Also, bubsizedis.exe crashes because there is too little RAM (Arbeitsspeicher). Did another run even though concentrations were a bit higher than usual (1/100 instead of 0.4/100). Quick post-processing showed that data set to be OK. The vacuum pump suddenly made a crushing noise, so I shut it down. The black tank was full, and had to be emptied. I was not 100% sure how to empty it, so I waited until Jimmy showed me how. It was as I thought it should. The vacuum pump sucked water from the tank in, which made it unusable for the day, as the hole where gas should be sucked in became wet.

22-03-2017

During first data collection of the day the vacuum pump started leaking water again due to water entrainment. Had to stop the experiment, call in for Jimmy for help, and watch him fix it and wait a little before being able to operate the system again. In order for all the water to come out, I was supposed to empty the tank (it was), and open this side valve at the vacuum pump in order for the air to push out all the water. Noted for next time this may happen. Different tdms measurements, as well as wms measurements at 40k 40k 10slpm. Processed WMS data at the same time in WMS Framework. I saw that 'error some Framen may be missing' indeed meant that some frames were partially missing. With that I mean that our resolution dropped from 64x64 to something like 59x61 or so.Liquid flow pipe A started shaking at higher liquid flow rates. I felt unsafe, so terminated the experiment.

23-03-2017

No test cases today. Made the matlab file more robust (for automation) and made figures for 4040, and 8080 cases. Still have to safe figures for 6060, but that's a matter of saving them basically.

24-03-2017

Tightened so that gas flux in A may diminish. It didn't, unfortunately. It was insignificant enough to pursue with the experiment. Some dye recirculated into the system, but data output showed it not affecting the measurements, fortunately. Further worked on making MATLAB code more robust. We replaced an outlet tube (upstream of the pump) with a valve and closed it off, because we saw air coming in from there. Turned on system again, no air anymore: problem solved.

27-03-2017

I apparently left the freshwater inlet valve open, which overflowed the tank during the weekend. Ellie and I worked on getting the tank clean that day, I removed a cracked flange (I tightened them too much the Friday before, which made it crack), and we assembled some parts of the sub-off (?) (that missile-looking construction). New parts for the flange will come in tomorrow, so that'll have to be fixed then. Hopefully we'll be able to run the facility by Wednesday again.

29-03-2017

Test case. Dye came back in.

30-03-2017

50 WMS measurements. E-mailed HZDR about WMS problems. Fixed problem by following his suggestions: take those cards in the WMS box in and out. Left drain valve open when I left that day.

31-03-2017

Tank is being refilled, because I left the drain valve open. Had a short talk with Jimmy about accountability. Took out the trash. Started WMS processing. Called Tectivity. E-mailed Tectivity. Worked on optimal flush and measurement times with the new volume of water that's in the tank. We started running the WMS data processing (40 data sets).

02-04-2017

Took four data sets: Re = [100k 100k] at 0, 10, 20, and 50 slpm gas flux. This was the first time we tried to take measurements with the tank almost completely filled. The wedges were lifted approximately 10 cm, we added a bit more chlorine, and we adjusted the times. All of that lead to a significant improvement in taking data: we took four sets in approx. 2.5 hours (one measurement takes 20 minutes, so set-up time (waiting for dye concentration to be low, gathering data from different PCs, and waiting for the system to arrive in a steady-state) was less than 1.5 hours. WMS data processing has still not finished.

03-04-2017

Took two data sets: Re = [100k 100k] at 100 and 150 slpm gas flux. WMS data processing finished today. It took an entire weekend to finish it, because bubsizedis.exe crashed a few times along the way, and if there's no one around to click ‘close program’ (so that the script can continue running) it just stays there waiting, doing nothing. Tried to redo some, to see whether they'd work this time, but they didn't, for some reason.

04-04-2017

Created all figures. Text - observations. Looked at what different Re and gas fluxes did to mixing.

05-04-2017

Conference paper and analysis

06-04-2017

Conference paper and analysis

07-04-2017

20 mm gap measurements

10-04-2017

Six 20 mm gap measurements

11-04-2017

20 mm gap measurements. Three new ones, and had to redo three, because fluorometer data was just too off.

12-04-2017

Spend the day trying to figure out why x and y differed so much. Thought I found some kind of an explanation (counter-intuitive pressure differences), until I looked at other data runs that contradict the hypothesis (or it could be the case that pressure readings from those other data sets were wrong, but that could also mean the more recent readings are wrong). I redid one data set that had large differences between x and y at Re = [40k x 40k]. The results were a lot worse than before: larger differences between x and y, while the pressure differences between the two channels were virtually zero.

13-04-2017

As I couldn't find any proper indications of why x and y differ so much at low Re, we'll just continue measuring data. Today: [80k 80k]. Perhaps it's really only existent at the lower Reynolds numbers. That fact would at least help us look in a certain direction. Took all [80k 80k] data. Redid 8080-100slpm. The second time the C7 values were quite off. Then, looking at the first 8080-100slpm run, we saw that it wasn't that steady there as well. We also noticed that the time needed for the sensor to read in a steady-state needs to be increased. As the 'looking for averages around points'-method to find this steady state time isn't reliable, we decided to hardcode a 50-second delay in there. Having said that, we now need to recreate the mixing figures we made.

14-04-2017

So today I'm changing those reading methods I talked about yesterday, and reproducing the figures, whilst making sure the C7 data is analyzed as to verify the soundness of the results we're seeing. Also, upon arriving at the lab the tank was pretty much empty. Strange, as all valves had been closed upon my leave the day before. There were still some tests going on after I left, so that may have caused it, I assume. This means that I will not be able to take any measurements today.

17-04-2017

Planning on redoing every single data set which shows to be incorrect for the fluorodata and then update the mixing figures they correspond to. These sets are: 2, 3, 4, 5, 21, 12, 32. Can't redo the first six, as they're taken at a gap height of 50 mm.

17-04-2017

Updated some data sets mixing data for as far I could manage.

24-04-2017

Worked on the presentation needed by [...].

25-04-2017

Looked at twelve cases of data at channel ai using the WMS and HSC.

26-04-2017

Imaging data. Code didn't work as we wanted, but we really needed data, so decided to take manual measurements of bubble sizes.

27-04-2017

Discussed what's important for the technical report, worked on a summary data table, added comments to MATLAB file

28-04-2017

FINAL DAY - final documentation, cleaning up, lunch with Jimmy

References

[1] Eifler, W. & Nijsing, R. 1967. Experimental investigation of velocity distribution and flow resistance in a triangular array of parallel rods. *Nuclear Engineering and Design*, 5, 22-42.

[2] Möller, S. V. 1991. On phenomena of turbulent flow through rod bundles. *Experimental Thermal and Fluid Science*, 4, 25-35.

[3] Meyer, L. & Rehme, K. 1994. Large-scale turbulence phenomena in compound rectangular channels. *Experimental Thermal and Fluid Science*, 8, 286-304.

[4] Krauss, T. & Meyer, L. 1998. Experimental investigation of turbulent transport of momentum and energy in a heated rod bundle. *Nuclear Engineering and Design*, 180, 185-206.

[5] Baratto, F. Bailey, S. C. C. & Tavoularis, S. 2006. Measurements of frequencies and spatial correlations of coherent structures in rod bundle flows *Nuclear Engineering and Design*, 236, 1830-1837.

[6] Merzari, E., Ninokata, H., Mahmood, A. & Rohde, M. 2009. Proper orthogonal decomposition of the flow in geometries containing a narrow gap *Theoretical and Computational Fluid Dynamics*, 23, 333-351.

[7] Mäkiharju, S. A., Ceccio, S. L., Buchanan, J. R., Mychkovsky, A. G., Hogan, K. J. & Lowe, K. T. 2015. Experimental Characterization of Interchannel Mixing Through a Narrow Gap. In *International Topical Meeting on Nuclear Reactor Thermal Hydraulics 2015*, NURETH 2015 (Vol. 5, pp. 4394–4409).

[8] Duret, B., Luret, G., Reveillon, J., Menard, T., Berlemont, A. & Demoulin, F. X. 2012. DNS analysis of turbulent mixing in twophase flows *International Journal of Multiphase Flow*, 40, 93-105.

[9] Meyer, L. 2010. From discovery to recognition of periodic large scale vortices in rod bundles as source of natural mixing between subchannels-A review. *Nuclear Engineering and Design*, 240, 1575–1588.

[10] Home, D., Arvanitis, G., Lightstone, M. F. & Hamed, M. S. 2009. Simulation of flow pulsations in a twin rectangular subchannel geometry using unsteady Reynolds Averaged Navier-Stokes modelling. In *Nuclear Engineering and Design* (Vol. 239, pp. 2964–2980).

[11] Derksen, J. J. 2010. Simulations of lateral mixing in crosschannel flow. *Computers and Fluids*, 39, 1058–1069.

[12] Chang, D. & Tavoularis, S. 2007. Numerical simulation of turbulent flow in a 37-rod bundle. *Nuclear Engineering and Design*, 237, 575–590.

[13] Chang, D. & Tavoularis, S. 2006. Convective Heat Transfer in Turbulent Flow Near a Gap. *Journal of Heat Transfer*, 128, 701.

[14] Pang, B. 2014. Numerical study of void drift in rod bundle with subchannel and CFD codes. doi:10.5445/KSP/1000041053

[15] Ko, J., Lucor, D. & Sagaut, P. 2008. Sensitivity of twodimensional spatially developing mixing layers with respect to uncertain inflow conditions. *Physics of Fluids*, 20. doi:10.1063/1.2937465

[16] Ito, D., Prasser, H. M., Kikura, H. & Aritomi, M. 2011. Uncertainty and intrusiveness of three-layer wire-mesh sensor. *Flow Measurement and Instrumentation*, 22, 249–256.

[17] Prasser, H.-M., Scholz, D. & Zippe, C. 2001. Bubble size measurement using wire-mesh sensors *Flow Measurement and Instrumentation*, 12/4. 299-312.

[18] Prasser, H.-M., Misawa, M. & Tiseanu, I. 2005. Comparison between wire-mesh sensor and ultra-fast X-ray tomograph for an air-water flow in a vertical pipe *Flow Measurement and Instrumentation*, 16, 73-83.

[19] Rohde, U.; Kliem, S.; Höhne, T.; Karlsson, R.; Hemström, B.; Lillington, J.; Toppila, T.; Elter, J.; Bezrukov, Y. 2005. Fluid mixing and flow distribution in the reactor circuit, measurement data base. *Nuclear Engineering and Design*, 235, 421-443